Data collection

During the follow-up period, patients visited the ICD outpatient clinic routinely every 3–6 months and were encouraged to seek additional visits whenever shocks, palpitations, syncope, or presyncope occurred. Devices were interrogated to analyze the number and type of episodes with stored electrograms on each visit. We used only one zone (VF zone) as a detection zone, and the detection heart rate setting of VF was programmed to 199 ± 10 bpm (median 200 bpm). We evaluated all appropriate shock episodes with an accurate time and date of the occurrence recorded by the ICD as VF episodes, and subsequent multiple ICD discharges within 1 week after one VF episode were eliminated to avoid any distortion of the data due to arrhythmic clusters with electrical instability. We also investigated the distributions of electrical storms. Electrical storms are usually defined as three or more appropriate shock episodes within 24 hours.[14] However, we tried to evaluate the daily distribution of electrical storms more precisely, and thus we defined electrical storms as three or more appropriate shock episodes within 4 hours. The onset of the electrical storm was defined as the first episode of the consecutive VF episodes.

For the purposes of this study, the seasons were defined as follows according to the Japanese seasons: winter = December to February; spring = March to May; summer = June to August; fall = September to November. In addition, the time of the day was classified into the following four 6-hour periods: midnight (0:00) to 6:00, 6:00 to noon (12:00), noon (12:00) to 18:00, and 18:00 to midnight (24:00).

Statistics

Quantitative data are presented as the mean ± standard deviation and were compared using a two-tailed Student's *t*-test. Categorical data are presented as absolute and percentage frequencies and were analyzed by the χ^2-test. The difference in the frequency of VF was analyzed by the goodness-of-fit test for the multinomial distribution. $P < .05$ was considered statistically significant.

Table 1 Clinical characteristics and follow-up data (n = 62)

Clinical characteristics:	
Age at ICD implantation, years	49 ± 14
Gender male/female (%)	58 (94)/4 (6)
Documentation of VF/CA/unknown syncope (%)	47/62 (76)
Family history of sudden cardiac death (%)	19/62 (31)
Induction of VF (%)	47/58 (81)
Follow-up:	
Follow-up duration after ICD implantation, months	70 ± 36
Patients with VF episodes during follow-up (%)	19/62 (31)
No. of isolated VF episodes (per patient)	98 (5.2 ± 4.0)
Patients with electrical storms during follow-up (%)	7/62 (11)

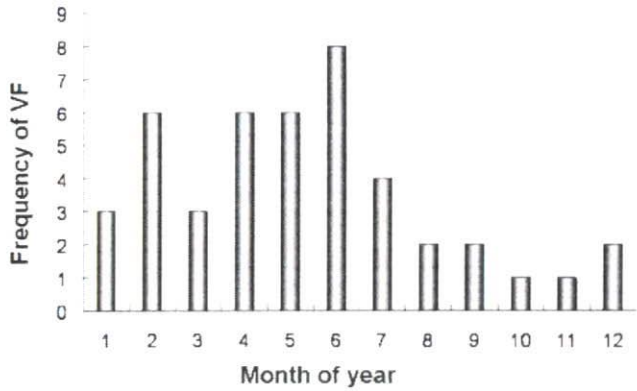

Figure 1 Monthly distribution of the first episodes of VF/CA/unknown syncope before ICD in patients with Brugada syndrome (n = 44). There was a seasonal peak from spring to early summer.

Results

Patient characteristics and VF episodes

Table 1 shows the clinical characteristics and follow-up data of the 62 patients with Brugada syndrome. Forty-seven (76%) patients had a history of VF/CA/unknown syncope. We could obtain the precise data of the first episodes of VF/CA/unknown syncope before implantation of ICD in 44 patients, and seasonal and circadian distributions of the first episodes of VF/CA/unknown syncope are shown in Figures 1 and 2. The seasonal distribution of the first episodes of VF/CA/unknown syncope indicated that there was a seasonal peak from spring to early summer. As for the diurnal distribution, there was a circadian peak from midnight to early morning. Familial history of sudden cardiac death was recognized in 19 patients. VF was induced by programmed electrical stimulation in 47 of 58 patients examined. SCN5A mutations accounted for seven out of the 62 study subjects.

During the follow-up period (17–175 months, median 64 months), 19 (31%) of the 62 patients had at least one episode of VF terminated by ICD therapy. There was no significant difference in the episodes of VF after ICD implantation between the two groups, patients with induced VF and patients without induced VF (34% vs. 27%; $P = .37$). Four patients were prescribed β-blockers due to neu-

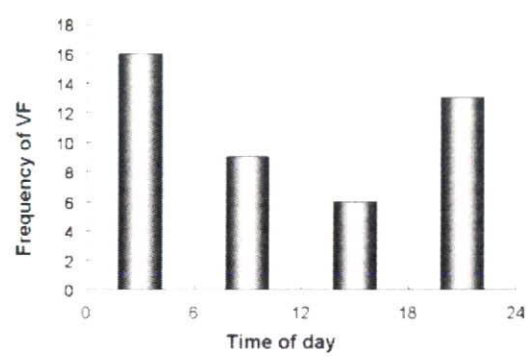

Figure 2 Circadian distribution of the first episodes of VF/CA/unknown syncope before ICD in patients with Brugada syndrome (n = 44). There was a circadian peak from midnight to early morning.

rally mediated syncope or inappropriate ICD therapy. However, there were no VF events during the follow-up period among these four patients.

The mean duration between the ICD implantation and first appropriate shock episode was 632 ± 692 days (median 250 days). Although a total of 180 appropriate shock episodes were recorded, 98 appropriate shock episodes were evaluated as isolated VF episodes (5.2 ± 4.0 per patient; median 4) since 82 episodes occurred within 1 week after one VF episode.

Seasonal distribution of VF

The monthly distribution of the 98 VF episodes recorded by ICDs is shown in Figure 3. The most frequent episodes of VF occurred in June (13 episodes); on the other hand, the fewest episodes of VF occurred in December (four episodes). The frequency of the VF among the 4-month periods was statistically different, and there was a significant peak between March and June ($P = .03$). In addition, the figure shows a small peak between September and October and a nadir between December and January. By a seasonal analysis, the highest number of VF episodes occurred from spring to early summer (44 episodes). Although not significant, there appeared to be the fewest from late fall to winter (23 episodes). The occurrence of VF from spring to early summer was 1.9 times as much as that from late fall to winter.

Circadian distribution of VF

Figure 4 shows the circadian distribution of the 98 VF episodes recorded by ICDs. The circadian distribution of the VF was statistically different among the four 6-hour periods, and there was a significant peak from midnight to 6:00 ($P < .0001$). When focusing on the daytime, there were small peaks from 7:00 to 9:00, 12:00 to 14:00, and 17:00 to 20:00, which were consistent with mealtimes or postprandial periods.

Electrical storm of VF

Seven (37%) of the19 patients experienced electrical storms of VF. Two patients had more than one episode of an electrical storm. Among a total of 10 electrical storms, five (50%) episodes occurred between May and June, which is shown in Figure 5. Regarding circadian variations, electrical storms were detected more frequently at night than during the daytime (Figure 6) and while sleeping than while awake.

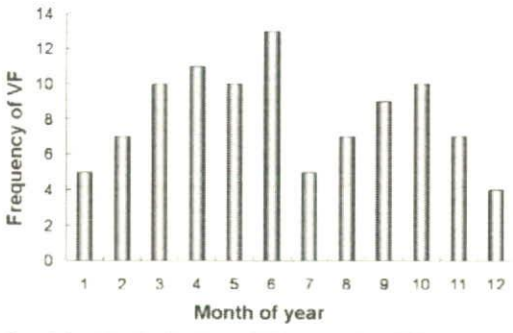

Figure 3 Monthly distribution of VF recorded by ICDs in patients with Brugada syndrome (n = 98). There was a significant peak between March and June.

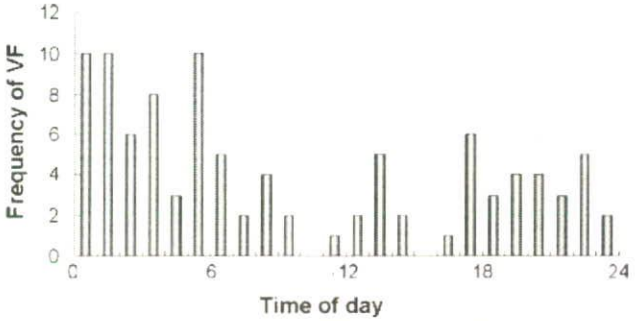

Figure 4 Circadian distribution of VF recorded by ICDs in patients with Brugada syndrome (n = 98). The occurrence of VF was significantly more frequent between midnight and 6:00 than during any other periods.

Nine (90%) episodes occurred at night (18:00–6:00), and only one (10%) episode occurred during the daytime (6:00–18:00). Seven (70%) episodes occurred while sleeping, and three (30%) episodes occurred while awake.

Discussion

Our study indicates that there are specific seasonal and circadian variations of the VF episodes in patients with Brugada syndrome, which are quite different from those observed in patients with structural heart disease. There was a significant seasonal peak from spring to early summer and a significant circadian peak from midnight to early morning. The seasonal and circadian variations of electrical storms were similar to those of isolated VF episodes. These findings could be related to the underlying pathophysiology of Brugada syndrome.

Possible mechanisms for seasonal distribution of VF

Muller et al[7] reported that there was a significant seasonal peak of VT/VF in the winter by analyzing appropriate ICD shock episodes in patients with structural heart disease. Arntz et al[8] also showed there was a seasonal variation in cardiac deaths, with a higher incidence in the winter. Although many investigators have documented that cardiac events including VT/VF in patients with structural heart disease increase significantly in the winter,[9,15–17] the highest num-

Figure 5 Monthly distribution of electrical storms recorded by ICDs in patients with Brugada syndrome (n = 10). More episodes of electrical storms occurred between the spring and early summer.

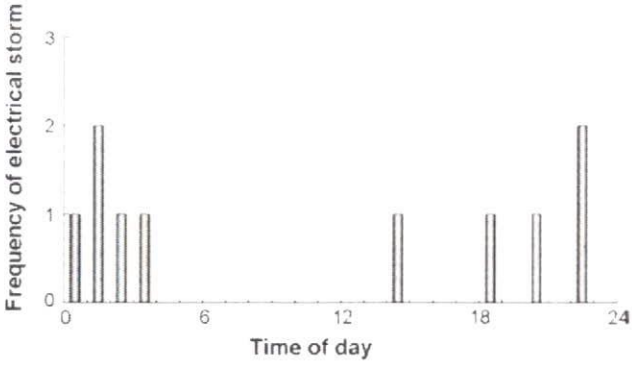

Figure 6 Circadian distribution of electrical storms recorded by ICDs in patients with Brugada syndrome (n = 10). Electrical storms were detected more frequently at night than during the daytime.

ber of VF episodes in the patients with Brugada syndrome occurred between spring and early summer. The underlying mechanisms for these seasonal distributions remain unclear. Although various environmental factors and physiological changes seem to play significant roles in the genesis of VF, hormonal activity, especially plasma catecholamine level, and autonomic nerve activity may explain the cause of these seasonal variations. Kruse et al[18] reported that plasma catecholamine level was the highest during the winter and the lowest during the summer. As for the pathogenesis of VF in patients with Brugada syndrome, α-adrenergic agonist and β-adrenergic blockers unmask a Brugada-type ECG and, moreover, could be related to the genesis of VF. The β-adrenergic agonists, on the other hand, are supposed to be protective in patients with Brugada syndrome by normalizing the ST segment and suppressing episodes of VF by increasing the $I_{Ca\text{-}L}$ current. In fact, several clinical studies have indicated the protective effects of β-adrenergic agonist in suppressing episodes of VF.[19–21] In terms of autonomic nerve activity, Krital-Boneh et al[22] suggested that vagal nerve activity was lower in the winter. Although it would be true that both hormonal activity and autonomic nerve activity could be somehow associated with occurrence of VF, physiological factors including levels of physical activity and behavioral changes such as eating or drinking and emotional factors also seem to be related to the occurrence of VF in patients with Brugada syndrome, and various environmental factors including temperature, air pressure, and humidity could be related to the VF occurrence. Most parts of Japan are visited by a rainy season from June to early July, which results in relatively stable bad weather with a lot of rain for several weeks. These weather conditions may be related to the high frequency of VF occurrence. It would be difficult to determine the independent factors responsible for the seasonal distributions of VF occurrence.

Possible mechanisms for circadian distribution of VF

There were certain circadian patterns of the occurrence of VF in the patients with Brugada syndrome. The episodes of ventricular tachyarrhythmias occurred most frequently between midnight and early morning, which was different from the previous reports on the patients with structural heart disease.[9–12] However, it was consistent with our previous data in a small population[13] and the other data on patients with Brugada syndrome.[4] A possible mechanism to explain the difference in the circadian patterns between the patients with organic heart disease and those with Brugada syndrome could be the effect of autonomic nervous activity. Sympathetic activity is supposed to be associated with the occurrence of VF in patients with organic heart disease. However, an increase of vagal activity plays a significant role in the genesis of VF in patients with Brugada syndrome. It is well-known that sympathetic nerve activity is higher during the daytime and upon awakening, whereas vagal nerve activity is higher during the night and upon sleeping.[23,24] There have been several studies showing the association between vagal nerve activity and the occurrence of VF in patients with Brugada syndrome.[25–28] Kasanuki et al[25] reported a sudden increase of vagal activity just before the episodes of VF in patients with Brugada syndrome. In an experimental study, Yan and Antzelevitch reported that vagal stimulation suppressed $I_{Ca\text{-}L}$ current leading to augmentation of ST-segment elevation.[29,30]

When focusing on the daytime, there were small peaks during mealtimes or postprandial periods. Nishizaki et al[31] showed that high insulin secretion induced by oral glucose intake was associated with augmentation of ST-segment elevation in patients with Brugada syndrome. Ikeda et al[32] reported a full stomach test as a novel diagnostic technique for identifying patients at risk for Brugada syndrome, and a positive test outcome was characterized by a high incidence of a history of life-threatening events. Mizumaki et al[33] indicated that augmentation of ST elevation was enhanced during the postprandial periods, especially after dinner, which could be related to the occurrence of VF in the late evening. All of these reports could indirectly support the increases in the occurrence of VF during the mealtime or postprandial periods in patients with Brugada syndrome.

Electrical storm

In the present study, the observations of the patients with Brugada syndrome indicated that more episodes of electrical storms occurred at night than during the daytime and between the spring and early summer than in any other seasons. Greene et al[34] reported a seasonal distribution of electrical storms in ICD patients with structural heart disease, in which the electrical storms occurred more frequently in the winter and less in the spring. As for the circadian variation of the electrical storms with structural heart disease, Englund et al[35] showed that there were distinct morning and afternoon peaks of arrhythmic storms of VT/VF, whereas the frequency of the electrical storm episodes exhibited a nadir at night. We also have preliminary data that the occurrence of electrical storms in patients with structural heart disease exhibited a significant peak from 6:00 to 11:00. The reason for this discrepancy of the occurrence of electrical storms between Brugada syndrome and structural heart disease could be, in part, similar to that of

the isolated VF episodes. However, further investigations with a larger population are needed.

Study limitations

First, regarding the distributions in the electrical storms of VF, the number of patients was too small to validate the present findings and to explain the underlying mechanisms. Therefore, further studies using a large number of patients are needed. Second, our study population showed male preponderance (94%), which may influence the results. Third, there could be an interindividual distortion. We thought that the interindividual distortion could be minimized by eliminating the multiple episodes within 1 week and recognizing the similar distributions of each patient's episodes. However, it is very important to evaluate whether the elimination of subsequent multiple ICD discharges within 1 week after one VF episode is adequate in Brugada syndrome when we investigate seasonal and circadian patterns of VF. We also investigated the seasonal and circadian distributions of all the episodes (n = 180), and we recognized that seasonal and circadian distributions of all of the 180 VF episodes are similar to those of isolated VF episodes.

Conclusion

In patients with Brugada syndrome, there was a significant seasonal peak from spring to early summer and a significant circadian peak from midnight to early morning in terms of the occurrences of VF.

Acknowledgments

We gratefully acknowledge the expert statistical assistance of Akiko Kada.

References

1. Brugada P, Brugada J. Right bundle branch block, persistent ST segment elevation and sudden cardiac death: a distinct clinical and electrocardiographic syndrome. A multicenter report. J Am Coll Cardiol 1992;20:1391–1396.
2. Gussak I, Antzelevitch C, Bjerregaard P, et al. The Brugada syndrome: clinical, electrophysiologic and genetic aspects. J Am Coll Cardiol 1999;33:5–15.
3. Wilde AA, Antzelevitch C, Borggrefe M, et al and the Study Group on the Molecular Basis of Arrhythmias of the European Society of Cardiology. Proposed diagnostic criteria for the Brugada syndrome: consensus report. Circulation 2002;106:2514–2519.
4. Antzelevitch C, Brugada P, Borggrefe M, et al. Brugada syndrome: report of the second consensus conference: endorsed by the Heart Rhythm Society and the European Heart Rhythm Association. Circulation 2005;111: 659–670.
5. Sacher F, Probst V, Iesaka Y, et al. Outcome after implantation of a cardioverter-defibrillator in patients with Brugada syndrome: a multicenter study. Circulation 2006;114:2317–2324.
6. Shimizu W, Aiba T, Kamakura S. Mechanisms of disease: current understanding and future challenges in Brugada syndrome. Nat Clin Pract Cardiovasc Med 2005;2:408–414.
7. Muller D, Lampe F, Wegscheider K, et al. Annual distribution of ventricular tachycardias and ventricular fibrillation. Am Heart J 2003;146:1061–1065.
8. Arntz HR, Willich SN, Schreiber C, et al. Diurnal, weekly and seasonal variation of sudden death. Population-based analysis of 24,061 consecutive cases. Eur Heart J 2000;21:315–320.
9. Anand K, Aryana A, Cloutier D, et al. Circadian, daily, and seasonal distributions of ventricular tachyarrhythmias in patients with implantable cardioverter-defibrillators. Am J Cardiol 2007;100:1134–1138.
10. Muller JE, Ludmer PL, Willich SN, et al. Circadian variation in the frequency of sudden cardiac death. Circulation 1987;75:131–138.
11. Willich SN, Levy D, Rocco MB, et al. Circadian variation in the incidence of sudden cardiac death in the Framingham Heart Study population. Am J Cardiol 1987;60:801–806.
12. Lampert R, Rosenfeld L, Batsford W, et al. Circadian variation of sustained ventricular tachycardia in patients with coronary artery disease and implantable cardioverter-defibrillators. Circulation 1994;90:241–247.
13. Matsuo K, Kurita T, Inagaki M, et al. The circadian pattern of the development of ventricular fibrillation in patients with Brugada syndrome. Eur Heart J 1999;20:465–470.
14. Ohgo T, Okamura H, Noda T, et al. Acute and chronic management in patients with Brugada syndrome associated with electrical storm of ventricular fibrillation. Heart Rhythm 2007;695–700.
15. Spencer FA, Goldberg RJ, Becker RC, et al. Seasonal distribution of acute myocardial infarction in the second National Registry of Myocardial Infarction. J Am Coll Cardiol 1998;31:1226–1233.
16. Page RL, Zipes DP, Powell JL, et al and the AVID Investigators. Seasonal variation of mortality in the Antiarrhythmics Versus Implantable Defibrillators (AVID) study registry. Heart Rhythm 2004;1:435–440.
17. Kloner RA, Poole WK, Perritt RL. When throughout the year is coronary death most likely to occur? A 12-year population-based analysis of more than 220 000 cases. Circulation 1999;100:1630–1634.
18. Kruse HJ, Wieczorek I, Hecker H, et al. Seasonal variation of endothelin-1, angiotensin II, and plasma catecholamines and their relation to outside temperature. J Lab Clin Med 2002;140:236–241.
19. Watanabe A, Fukushima Kusano K, et al. Low-dose isoproterenol for repetitive ventricular arrhythmia in patients with Brugada syndrome. Eur Heart J 2006;27: 1579–1583.
20. Bonnemeier H, Richardt G, Potratz J, et al. Circadian profile of cardiac autonomic nervous modulation in healthy subjects: differing effects of aging and gender on heart rate variability. J Cardiovasc Electrophysiol 2003;14:791–799.
21. Shimizu W, Kamakura S. Catecholamines in children with congenital long QT syndrome and Brugada syndrome. J Electrocardiol 2001;34:173–175.
22. Kristal-Boneh E, Froom P, Harari G, et al. Summer-winter differences in 24 h variability of heart rate. J Cardiovasc Risk 2000;7:141–146.
23. Trinder J, Kleiman J, Carrington M, et al. Autonomic activity during human sleep as a function of time and sleep stage. J Sleep Res 2001;10: 253–264.
24. Shinar Z, Akselrod S, Dagan Y, et al. Autonomic changes during wake-sleep transition: a heart rate variability based approach. Auton Neurosci 2006;130:17–27.
25. Kasanuki H, Ohnishi S, Ohtuka M, et al. Idiopathic ventricular fibrillation induced with vagal activity in patients without obvious heart disease. Circulation 1997;95:2277–2285.
26. Miyazaki T, Mitamura H, Miyoshi S, et al. Autonomic and antiarrhythmic drug modulation of ST segment elevation in patients with Brugada syndrome. J Am Coll Cardiol 1996;27:1061–1070.
27. Noda T, Shimizu W, Taguchi A, et al. ST-segment elevation and ventricular fibrillation without coronary spasm by intracoronary injection of acetylcholine and/or ergonovine maleate in patients with Brugada syndrome. J Am Coll Cardiol 2002;40:1841–1847.
28. Van den Berg MP, Haaksma J, Veeger NJ, et al. Diurnal variation of ventricular repolarization in a large family with LQT3-Brugada syndrome characterized by nocturnal sudden death. Heart Rhythm 2006;3:290–295.
29. Yan GX, Antzelevitch C. Cellular basis for the Brugada syndrome and other mechanisms of arrhythmogenesis associated with ST-segment elevation. Circulation 1999;100:1660–1666.
30. Antzelevitch C, Brugada P, Brugada J, et al. Brugada syndrome. A decade of progress. Circ Res 2002;91:1114–1118.
31. Nishizaki M, Sakurada H, Ashikaga T, et al. Effects of glucose-induced insulin secretion on ST segment elevation in the Brugada syndrome. J Cardiovasc Electrophysiol 2003;14:243–249.
32. Ikeda T, Abe A, Yusu S, et al. The full stomach test as a novel diagnostic technique for identifying patients at risk of Brugada syndrome. J Cardiovasc Electrophysiol 2006;17:602–607.
33. Mizumaki K, Fujiki A, Nishida K, et al. Postprandial augmentation of bradycardia-dependent ST elevation in patients with Brugada syndrome. J Cardiovasc Electrophysiol 2007;18:839–844.
34. Greene M, Newman D, Geist M, et al. Is electrical storm in ICD patients the sign of a dying heart? Outcome of patients with clusters of ventricular tachyarrhythmias. Europace 2000;2:263–269.
35. Englund A, Behrens S, Wegscheider K, et al. Circadian variation of malignant ventricular arrhythmias in patients with ischemic and nonischemic heart disease after cardioverter defibrillator implantation. European 7219 Jewel Investigators. J Am Coll Cardiol 1999;34:1560–1568.

Circ J 2008; **72:** 1705–1706

Mutation Analysis of the Glycerol-3 Phosphate Dehydrogenase-1 Like (*GPD1L*) Gene in Japanese Patients With Brugada Syndrome

Takeru Makiyama, MD; Masaharu Akao, MD; Yoshisumi Haruna, MD; Keiko Tsuji, MS*; Takahiro Doi, MD; Seiko Ohno, MD; Yukiko Nishio, MD; Toru Kita, MD; Minoru Horie, MD*

Brugada syndrome is an inherited arrhythmic disorder, and mutations in the *SCN5A* gene, encoding cardiac sodium channels, are identified in approximately 15% of cases. A novel causative gene (glycerol-3 phosphate dehydrogenase-1 like; *GPD1L*) has been reported, and in the present study, 80 unrelated Japanese patients were screened for *GPD1L* mutations: 1 synonymous mutation was identified, as well as 1 intronic variant, both of which were absent in 220 control alleles. Additionally, a single-nucleotide polymorphism was detected in 4 patients. No non-synonymous mutations were found. *GPD1L* does not appear to be a major cause of Brugada syndrome in the Japanese population. (*Circ J* 2008; **72:** 1705–1706)

Key Words: Arrhythmia; Brugada syndrome; *GPD1L*

Brugada syndrome (BrS) is an inherited disorder, characterized by sudden death from ventricular tachyarrhythmias and ST-segment elevation in the right precordial leads[1]. In approximately 15% of patients, loss-of-function mutations in the *SCN5A* gene, which encodes the α-subunit of the voltage-gated cardiac sodium channel, have been identified;[2] however, other responsible genes remain to be determined.

Recently, London et al identified a new causative gene, glycerol-3 phosphate dehydrogenase-1 like (*GPD1L*), using linkage analysis of a large Italian-descent family.[3] *GPD1L* mutations were found in patients with sudden infant death syndrome[4] but London's group did not identify *GPD1L* mutations in the probands of 19 smaller families with BrS.[3] Other investigators also failed to detect *GPD1L* mutations in 38 Dutch BrS patients.[5]

BrS is more prevalent in Asian countries, including Japan,[6] and we previously reported genetic analysis in 38 Japanese BrS patients.[7] We therefore screened extensively for the prevalence of *GPD1L* and *SCN5A* mutations in 80 Japanese probands with BrS in the present study, which was approved by the Institutional Ethics Committee and all patients provided informed consent.

The cohort consisted of 76 males and 4 females (mean age, 47.4±17.0 years); 39 patients (48.9%) were symptomatic and 26 (32.5%) had a family history of sudden death. The entire *GPD1L* coding region was amplified by each exon, and analyzed by denaturing high-performance liquid chromatography (Table 1).

We identified *SCN5A* mutations in 8 of the 80 patients (10%). Regarding *GPD1L* mutation analysis, we identified 1 synonymous mutation, c.465C>T (p.A155A), as well as 1 intronic variant, 48-30T>C, which were not present in 220 control alleles (Fig 1A). Neither of the probands experienced syncopal episodes nor did they have a family history of sudden death. However, both of them underwent implantable cardioverter defibrillator implantation because of inducible ventricular fibrillation during electrophysiological studies. Additionally, we detected a single-nucleotide polymorphism (*21G>T) in the 3'UTR in 4 patients (Fig 1A). The allele frequency of *21G>T in BrS patients (4/160) was not significantly different from that of normal controls (11/220). None of the *GPD1L*-variant carriers had *SCN5A* mutations. Fig 1B is a schematic of *GPD1L* and the location of the identified variants. Synonymous mutations and intronic variants might influence the splicing of exons and thereby cause various human diseases;[8] so we examined whether these variants might be predicted to cause splicing abnormality, using the splice-site prediction web interface (http://www.fruitfly.org/index.html). The variants did not change the scores of the splice donor or acceptor sites, suggesting they are unlikely to affect the splicing of *GPD1L*.

Recently, Antzelvitch et al reported that L-type cardiac calcium-channel gene mutations cause a specific type of BrS associated with short QT syndrome.[9] Koopmann et al investigated a number of candidate genes (*GPD1L*, Caveolin-3, *Irx-3*, *Irx-4*, *Irx-5*, *Irx-6*, *Plakoglobin*, *Plakophilin-2*, *SCN1B*, *SCN2B*, *SCN3B*, and *SCN4B*) in 38 Dutch BrS patients, but no mutations were found.[5] Despite enormous efforts, the genetic cause of the majority of BrS patients remains unknown. Nongenetic factors or unrecognized environmental factors may be responsible, but further studies are needed.

In conclusion, the present data suggest that the *GPD1L* does not appear to be a major cause of BrS in the Japanese

(Received May 29, 2008; revised manuscript received July 7, 2008; accepted July 9, 2008; released online September 2, 2008)

*Department of Cardiovascular Medicine, Kyoto University Graduate School of Medicine, Kyoto, *Department of Cardiovascular and Respiratory Medicine, Shiga University of Medical Science, Otsu, Japan*
Mailing address: Masaharu Akao, MD, Department of Cardiovascular Medicine, Kyoto University Graduate School of Medicine, 54 Kawahara-cho, Shogoin, Sakyo-ku, Kyoto 606-8507, Japan. E-mail: akao@kuhp.kyoto-u.ac.jp

Table 1 ***GPD1L*** **Primer Sequences and DHPLC Analysis Conditions**

Exon	*Forward primer sequence*	*Reverse primer sequence*	*PCR annealing temp (°C)*	*DHPLC temp (°C)*
1	*ACGGTCCAGGCGGCTACATT*	*GCAAGCAGGTGGCTTCTGTG*	*61.8*	*66*
2	*CTCTCCCGCCCAAGTGAGTT*	*CCAAGTGCTGCTCAGCCAAG*	*62*	*57, 65.3*
3	*CCTTGTGGACAGGCAAGGTT*	*TGTCTAGCCCTGGGCAGCAT*	*62*	*61.2, 62.5*
4	*GGCGGTTTGTTCTCTCCTAA*	*TAAGAGGGACAGGGAAGAGT*	*62*	*61.4*
5	*TCCTTGTTGTCTAACCTTTC*	*TGATGAACTCCTCCCCTGAG*	*56*	*60, 61*
6	*GGTGCTGTAACGGCATCT*	*CCAAGCCAGGAGTCTCAAGT*	*62*	*62.8, 64.5*
7	*TCTTTAGTCTTTACCATAGT*	*ATAGGAATGATGGACATTTA*	*50*	*57.5, 60.5, 61.5*
8	*CCAGTGGCCTAACTTTGTCT*	*ACTGCCCAGTACATCTTTGC*	*56*	*58, 59*

GPD1L, glycerol-3 phosphate dehydrogenase-1 like; DHPLC, denaturing high-performance liquid chromatography; PCR, polymerase chain reaction.

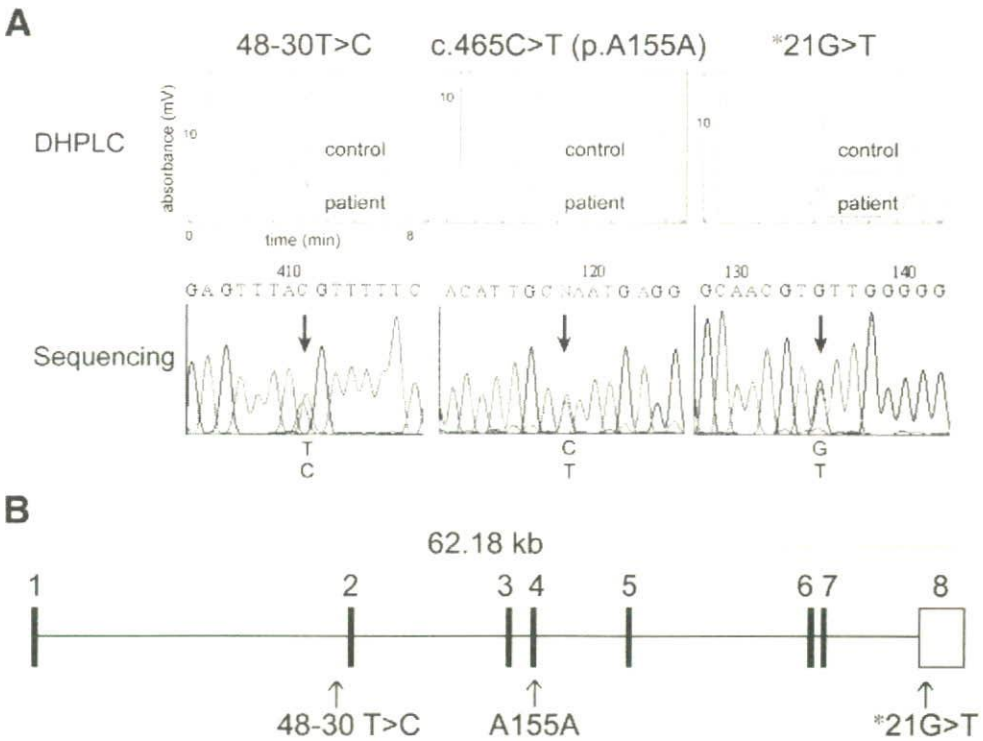

Fig 1. Genetic analysis and schematic representation of glycerol-3 phosphate dehydrogenase-1 like gene. (A) Denaturing high-performance liquid chromatography (DHPLC) elution profiles (Upper) and DNA sequencing electropherograms (Lower). (B) Exons and introns are shown as boxes and lines, and coding and non-coding regions are indicated by closed and open boxes, respectively.

population.

References

1. Brugada P, Brugada J. Right bundle branch block, persistent ST segment elevation and sudden cardiac death: A distinct clinical and electrocardiographic syndrome: A multicenter report. *J Am Coll Cardiol* 1992; **20:** 1391–1396.
2. Chen Q, Kirsch GE, Zhang D, Brugada R, Brugada J, Brugada P, et al. Genetic basis and molecular mechanism for idiopathic ventricular fibrillation. *Nature* 1998; **392:** 293–296.
3. London B, Michalec M, Mehdi H, Zhu X, Kerchner L, Sanyal S, et al. Mutation in glycerol-3-phosphate dehydrogenase 1 like gene (GPD1-L) decreases cardiac Na+ current and causes inherited arrhythmias. *Circulation* 2007; **116:** 2260–2268.
4. Van Norstrand DW, Valdivia CR, Tester DJ, Ueda K, London B, Makielski JC, et al. Molecular and functional characterization of novel glycerol-3-phosphate dehydrogenase 1 like gene (GPD1-L) mutations in sudden infant death syndrome. *Circulation* 2007; **116:** 2253–2259.
5. Koopmann TT, Beekman L, Alders M, Meregalli PG, Mannens MM, Moorman AF, et al. Exclusion of multiple candidate genes and large genomic rearrangements in SCN5A in a Dutch Brugada syndrome cohort. *Heart Rhythm* 2007; **4:** 756–757.
6. Hiraoka M. Brugada syndrome in Japan. *Circ J* 2007; **71**(Suppl): A-61–A-68.
7. Makiyama T, Akao M, Tsuji K, Doi T, Ohno S, Takenaka K, et al. High risk for bradyarrhythmic complications in patients with Brugada syndrome caused by SCN5A gene mutations. *J Am Coll Cardiol* 2005; **46:** 2100–2106.
8. Wang GS, Cooper TA. Splicing in disease: Disruption of the splicing code and the decoding machinery. *Nat Rev Genet* 2007; **8:** 749–761.
9. Antzelevitch C, Pollevick GD, Cordeiro JM, Casis O, Sanguinetti MC, Aizawa Y, et al. Loss-of-function mutations in the cardiac calcium channel underlie a new clinical entity characterized by ST-segment elevation, short QT intervals, and sudden cardiac death. *Circulation* 2007; **115:** 442–449.

J Pharmacol Sci **108**, 462 – 471 (2008)

Journal of Pharmacological Sciences

Full Paper

Hydroxyzine, a First Generation H_1-Receptor Antagonist, Inhibits Human Ether-a-go-go–Related Gene (HERG) Current and Causes Syncope in a Patient With the HERG Mutation

Tomoko Sakaguchi[1], Hideki Itoh[1], Wei-Guang Ding[2], Keiko Tsuji[1], Iori Nagaoka[1], Yuko Oka[1], Takashi Ashihara[1], Makoto Ito[1], Yoshihiro Yumoto[3], Naoko Zenda[4], Yukei Higashi[4], Youichi Takeyama[4], Hiroshi Matsuura[2], and Minoru Horie[1,*]

[1]*Department of Cardiovascular Medicine,* [2]*Division of Physiology, Shiga University of Medical Science, Otsu 520-2192, Japan*

[3]*Department of Cardio-Angiology, Kitasato University School of Medicine, Sagamihara 228-8555, Japan*

[4]*Division of Cardiology, Showa University Fujigaoka Hospital, Yokohama 227-8501, Japan*

Received July 4, 2008; Accepted October 14, 2008

Abstract. QT prolongation, a risk factor for arrhythmias, can result from genetic variants in one (or more) of the genes governing cardiac repolarization as well as intake of drugs known to affect a cardiac K^+ channel encoded by human ether-a-go-go–related gene (HERG). In this paper, we will report a case of drug-induced long QT syndrome associated with an H_1-receptor antagonist, hydroxyzine, in which a mutation was identified in the HERG gene. After taking 75 mg of hydroxyzine for several days, a 34-year-old female began to experience repetitive syncope. The deleterious effect of hydroxyzine was suspected because QTc interval shortened from 630 to 464 ms after cessation of the drug. Later on, the patient was found to harbor an A614V-HERG mutation. By using the patch-clamp technique in the heterologous expression system, we examined the functional outcome of the A614V mutation and confirmed a dominant-negative effect on HERG expression. Hydroxyzine concentration-dependently inhibited both wild-type (WT) and WT/A614V-HERG K^+ currents. Half-maximum block concentrations of WT and WT/A614V-HERG K^+ currents were 0.62 and 0.52 μM, respectively. Thus, accidental combination of genetic mutation and intake of hydroxyzine appeared to have led to a severe phenotype, probably, syncope due to torsade de pointes.

Keywords: hydroxyzine, QT prolongation, human ether-a-go-go–related gene (HERG), potassium channel, torsade de pointes

Introduction

A number of drugs prolonging QT interval have been shown to inhibit human ether-a-go-go–related gene (HERG) currents (1), and this fact was noted in the heterologously reconstituted HERG channels in a mammalian cell line. Terfenadine and astemizole are H_1-receptor antagonists that were shown to block HERG channels (2 – 4) and have been withdrawn from the market because of reported torsade de pointes (TdP) (5 – 9). We recently experienced a case with repetitive syncope after taking a first generation H_1-receptor blocker, hydroxyzine. The index patient was later found to have a heterozygous HERG mutation, A614V. As newer classes of H_1-receptor blockers were shown to inhibit HERG channels, we examined whether therapeutic concentrations of hydroxyzine also affect reconstituted wild type (WT) and mutant HERG channels using a heterologous expression system with Chinese hamster ovary (CHO) cells. The A614V mutant channels were nonfunctional and showed dominant-negative suppressions on WT HERG channel expression. The mutant subunit was refractory to the intracellular trafficking and this was the major mechanism for the

*Corresponding author. horie@belle.shiga-med.ac.jp
Published online in J-STAGE on December 5, 2008 (in advance)
doi: 10.1254/jphs.08178FP

reduced K^+ conductance. The therapeutic concentration range of hydroxyzine inhibited both WT channels and those expressing equimolar WT and mutant clones (mimicking heterozygous condition) at similar half-inhibiting concentrations. These findings indicated that the first generation H_1-blocker hydroxyzine also has a potential to induce QT prolongation, especially in the presence of other triggering factors such as genetic variants and hypokalemia.

Materials and Methods

Genomic DNA isolation and mutation analysis

Genomic DNA was prepared from peripheral blood leukocytes by using QIAamp DNA Blood Midi Kits (Qiagen, Valencia, CA, USA). All exons of the *HERG*, *KCNQ1*, *SCN5A*, *KCNE1*, *KCNE2*, and *KCNJ2* genes were amplified by PCR using intronic primer sequences. Genetic screening was performed by denaturing high performance liquid chromatography (DHPLC) using a WAVE System Model 3500 (Transgenomic, Omaha, NE, USA). Abnormal conformers were amplified by PCR and sequencing was performed on an ABI PRISM 3130 DNA sequencer (Applied Biosystems, Foster City, CA, USA).

Site-directed mutagenesis and expression, cell culture and transfection

Complementary DNAs (cDNAs) for *HERG* (GenBank AF363636) were kind gifts from Dr. M. Sanguinetti (University of Utah, Salt Lake City, UT, USA). The cDNA was subcloned into the pRcCMV plasmid (Invitrogen, Carlsbad, CA, USA) via pBluescript II KS(+) (Stratagene, La Jolla, CA, USA) (pRcCMV/WT-*HERG*). Site-directed mutagenesis of *HERG* was performed by an overlap extension PCR strategy. Nucleotide sequence analysis was performed on each variant construct before the expression study.

CHO cells were maintained in Dulbecco's modified Eagle medium and Ham's F12 nutritional mixture (Gibco-BRL, Rockville, MD, USA) supplemented with 10% fetal bovine serum (Gibco-BRL) and antibiotics (100 U/ml penicillin and 100 μg/ml streptomycin) in a humidified incubator gassed with 5% CO_2 and 95% air at 37°C. The cells were transiently transfected with either pRcCMV/HERG (WT and/or mutant) or pIRES-CD8/KCNQ1 + pIRES-CD8/KCNE1 using the LipofectAMINE method according to the manufacturer's instructions (Invitrogen). The amount of plasmids was 1 or 2 and 0.5 μg of GFP for a 35-mm dish, and only GFP-positive cells were used for the patch-clamp study.

Electrophysiological experiments

At 24 – 48 h after transfection, whole-cell patch-clamp recordings were conducted at 37 ± 1°C using an EPC-8 patch-clamp amplifier (HEKA, Lambrecht, Germany). No leak subtraction was used. The normal Tyrode solution contained 140 mM NaCl, 5.4 mM KCl, 1.8 mM $CaCl_2$, 0.5 mM $MgCl_2$, 0.33 mM NaH_2PO_4, 5.5 mM glucose, and 5 mM HEPES (pH adjusted to 7.4 with NaOH). The pipette solution contained 70 mM potassium aspartate, 40 mM KCl, 10 mM KH_2PO_4, 5 mM EGTA, 1 mM $MgSO_4$, 3 mM Na_2-ATP (Sigma Chemical Co., St. Louis, MO, USA), 0.1 mM Li_2-GTP (Roche Diagnostics GmbH, Mannheim, Germany), and 5 mM HEPES (pH adjusted to 7.4 with KOH). Hydroxyzine (Sigma) was dissolved in dimethyl-sulfoxide as a stock solution at a concentration of 100 mM and was kept in the dark at −20°C. Fresh drug solutions were prepared from the stock solutions immediately before use.

Whole-cell membrane current was recorded using the whole-cell configuration of the patch-clamp technique with an EPC-8 amplifier (HEKA). A coverslip with adherent CHO cells was placed on the glass bottom of a recording chamber (0.5 ml in volume) mounted on the stage of an inverted microscope (TE2000-U; Nikon, Tokyo). Pipette resistance was 3 – 5 MΩ when filled with internal solution. Currents and voltages were digitized and voltage commands were generated through an LIH-1600 AD/DA interface (HEKA) controlled by PatchMaster software (HEKA). Current amplitude was divided by membrane capacitance (Cm) to obtain current densities (pA/pF) in each cell. The voltage-dependence of current activation was determined by fitting the normalized tail current (I_{tail}) versus test potential (V_{test}) to a Boltzmann function expressed by the following equation: $I_{tail} = 1 / (1 + \exp[(V_{0.5} - V_t) / k])$, where $V_{0.5}$ is the voltage at which the current is half-maximally activated and k is the slope factor.

When we analyze steady-state inactivation, the corrected steady-state inactivation curves were fitted with a Boltzmann function in the following form:

$I / (I_{max} - I_{min}) = 1 / \{1 + \exp[(V_t - V_{0.5}) / k]\} + I_{min}$, where I is the amplitude of inactivating current corrected for deactivation, I_{max} is the maximum of I, I_{min} is the minimum of I, V_t is the prepulse of test potential, $V_{0.5}$ is the voltage at which I is half of I_{max}, and k is the slope factor.

Data analyses

Numerical data are presented as mean ± S.E.M. Student's t-test was used to compare the data between different groups for electrophysiological measurements, and differences were considered significant at $P<0.05$.

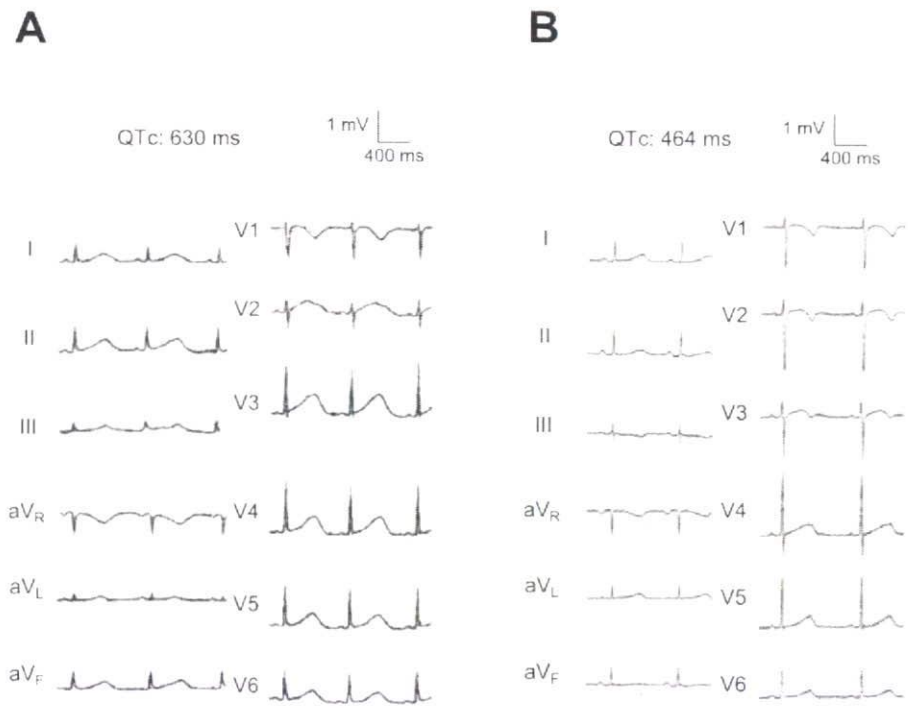

Fig. 1. Twelve-lead ECG traces. A: ECG the next day after syncope. B: ECG three weeks after discontinuing hydroxyzine.

Cell preparation and confocal imaging

For confocal microscopy experiments, green fluorescent protein (GFP) was tagged to the C terminus of WT or A614V HERG using EGFP-N1 vector (Clontech, Mountain View, CA, USA). HEK293 cells were plated on 35-mm glass-bottom culture dishes and maintained for 12 – 24 h in Dulbecco's modified Eagle's medium containing 10% FBS. Lipofection was performed with Lipofectamine reagent (Invitrogen). At 48 h after transfection, HEK293 cells were incubated for 15 – 18 h with 50 μM cycloheximide. The localization of GFP-tagged proteins was detected using an LSM 510-META laser-scanning microscope (Carl Zeiss, Thornwood, NY, USA) with a 63 × 1.40 numerical aperture oil-immersion objective (10). GFP was excited using a 488-nm line of an argon laser and signals were collected through a 500 – 530 band-pass filter.

Results

Case presentation

For the treatment of chronic pruligo, the 34-year-old woman began to take hydroxyzine (75 mg/day) and 3 days later, she experienced repetitive syncope. On admission, her ECG showed a marked QT prolongation (640 ms, QT_c = 630 ms; Fig. 1A), and her syncope was suspected to be due to TdP. She had no particular family history, but once had a pre-syncopal attack of unknown origin several years ago. Immediately after admission, hydroxyzine intake was stopped, and she was free of syncope since then. QT intervals gradually shortened to 460 ms (QT_c = 464 ms) three weeks after the episode (Fig. 1B). It was therefore evident that the drug induced an extreme prolongation of QT interval.

Because her QT interval remained slightly prolonged after the cessation of hydroxyzine, we conducted genetic testing and identified a heterozygous missense HERG mutation, A614V, causing a substitution of alanine at codon 614 to valine (Fig. 2: A – C). Panel A of Fig. 2 depicts the original results of screening by DHPLC, and panel B shows the DNA sequence data. Panel C shows her family tree; her two children were negative for this mutation. There was a heterozygous substitution of C to T at position 1841 in exon 7, which resulted in A614V. The mutation is located in the pore region (Fig. 2D) and has been known as a hot spot for the congenital LQTS (11 – 13).

Biophysical assay of wild type and mutant HERG channel function

In order to clarify the mechanism underlying the marked QT prolongation and syncope presumably due to TdP after intake of hydroxyzine, we conducted electrophysiological experiments by using CHO cells express-

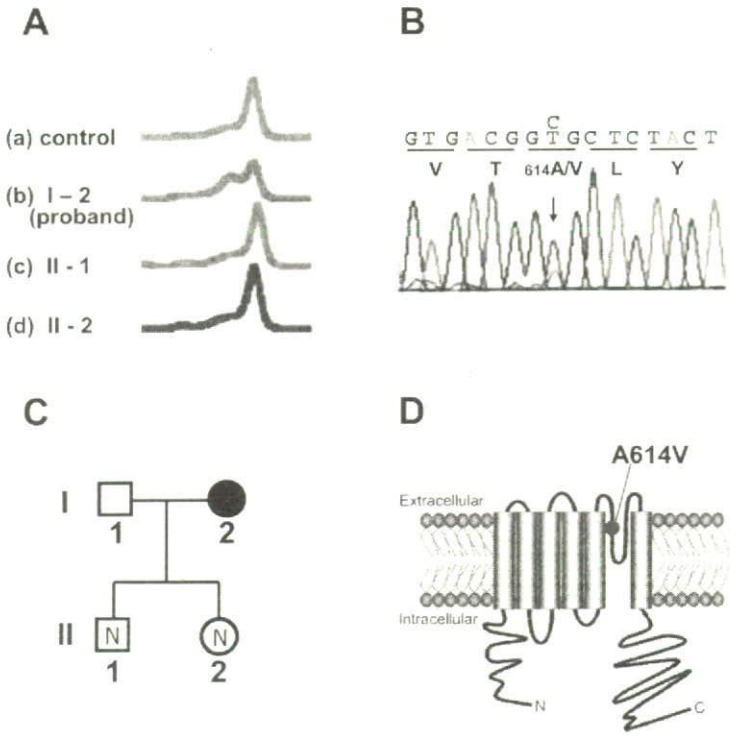

Fig. 2. Genetic testing revealed that the index patient had a missense HERG mutation. A: DHPLC analysis of PCR products of family members: from top to bottom, a: control, b: proband, c: her son, d: her daughter. The control, her son, and her daughter displayed one normal peak pattern, but the proband, in contrast, showed a two-peak pattern. B: Sequence identification of a C to T transition of one HERG allele in the proband (both alleles shown), causing replacement of alanine 614 by valine (A614V). C: Partial pedigree of the family (squares indicate men and circles, women). Filled symbol depicts mutation carrier and symbols with N, non-carriers; open symbol, family member without available findings. D: Schematic representation of the predicted topology of the HERG protein and the location of A614V. C = C-terminal domain and N = N-terminal domain.

ing either WT or mutant HERG channel. Figure 3A shows four sets of representative current traces recorded from CHO cells transfected with WT (2 and 1 μg, panels a and b), A614V alone (2 μg, panel c), or WT/A614V (1 μg each, panel d). Depolarization pulses applied from a holding potential of –80 mV to various test potentials elicited time-dependent outward K^+ currents, followed by the decaying outward tail current upon return to –60 mV in cells expressing WT HERG (Fig. 3A, panels a and b). In contrast, cells expressing A614V-HERG alone did not produce any measurable currents (Fig. 3A, panel c). When expressed with WT and A614V cDNA at 1:1 ratio, cells displayed significantly smaller outward currents compared with that of WT 1 μg (Fig. 3A, panel d).

As illustrated in Fig. 3B, the HERG-related K^+ currents were activated at potentials positive to –40 mV. The amplitude of outward current was increased with depolarization up to 0 mV, but was then progressively decreased with further depolarization, which is typical for an inward rectifying property of hERG (14). Therefore, when values for the maximum peak of steady state current during depolarizing pulses were plotted as a function of test potentials (Fig. 3B), the I-V curve showed a bell-shaped relation. Compared to the case of WT (1 μg, open squares, Fig. 3B), WT/A614V HERG channel (filled diamonds) displayed nearly 70% reduction in current density.

Peak tail currents elicited on repolarization to –60 mV from various test potentials were measured and then normalized by the cell capacitance in multiple cells. These values were plotted as a function of test potentials (Fig. 3C) and fitted with a Boltzmann equation, yielding half maximum activation potential ($V_{0.5}$) and slope factor (k) (Table 1). Maximum peak current densities measured at +50 mV in WT-HERG channels were 43.2 ± 4.0 and 29.4 ± 3.4 pA/pF (2 and 1 μg, respectively). In contrast, those in the WT/A614V-HERG channels were 7.9 ± 1.1 pA/pF and were significantly smaller (approximately one fourth) than those of the 1 μg WT channels. However, co-expression of A614V did not significantly alter $V_{0.5}$ and k values (Table 1). Thus, A614V appeared to cause a dominant-negative suppression on WT-HERG channel subunits without affecting the kinetic parameters.

We examined steady-state inactivation using a dualpulse protocol (Fig. 3D). There was no significant change in its voltage dependence between WT and WT/A614V. $V_{0.5}$ and the slope factor of steady-state inactivation were not different between WT and WT/A614V [$V_{0.5}$: –51.0 ± 2.8 for WT (n = 6), –54.4 ± 2.3 for WT/A614V (n = 7); slope factor: –27.4 ± 1.6 for WT, –26.3 ± 5.1 for WT/A614V].

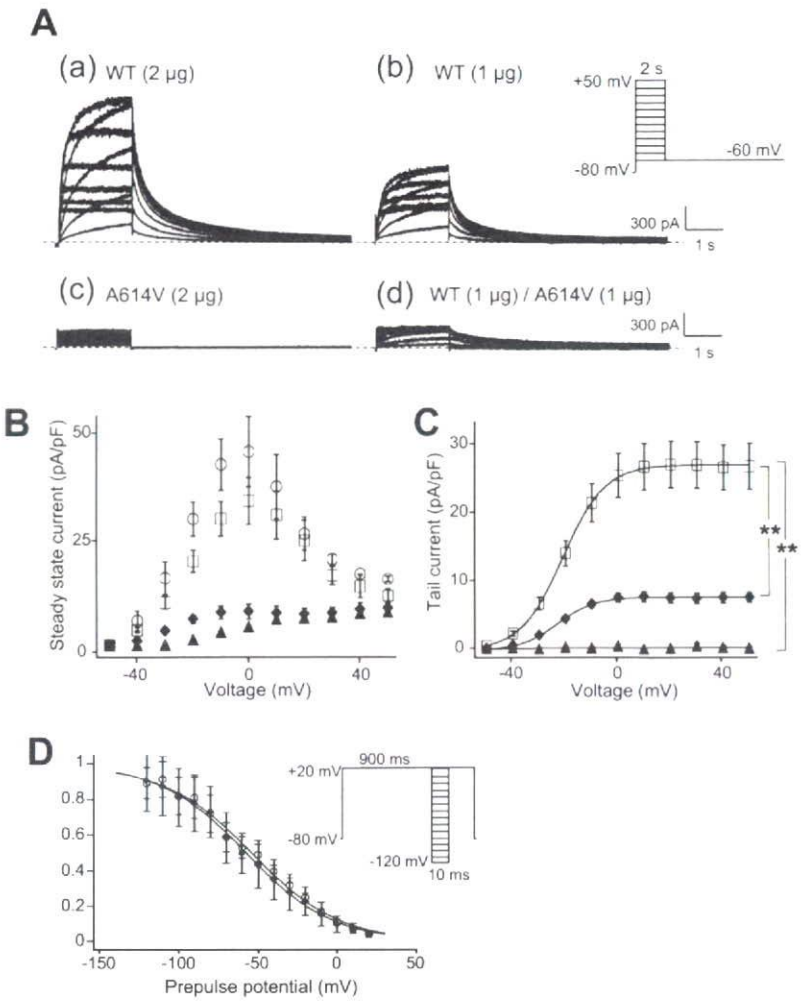

Fig. 3. Functional assays of A614V HERG channel in CHO cells. A: Representative current traces recorded from cells expressing the constructs indicated above each graph. Currents were elicited from a holding potential of −80 mV, by depolarizing pulses from −50 to +50 mV (with a 10-mV step increment) and subsequent repolarization to −60 mV. B: Steady state current–voltage relationships for WT-HERG (2 μg; open circles, n = 26), WT-HERG (1 μg; open squares, n = 22), A614V/WT-HERG (filled diamonds, n = 21), and A614V-HERG (filled triangles, n = 8). C: Tail current–voltage relations for WT-HERG (1 μg; open squares, n = 22), A614V/WT-HERG (filled diamonds, n = 21), and A614V-HERG (filled triangles, n = 8). **P<0.01 *vs* WT-HERG (1 μg). D: Normalized steady-state inactivation curves of expressed currents in CHO cells transfected with WT-HERG (open circles, n = 6) or A614V/WT-HERG (filled diamonds, n = 7). To examine the steady-state inactivation, conditioning pulses between −120 and +20 mV in 10-mV increments for 10 ms were applied after a depolarizing pulse to +20 mV for 900 ms, followed by a common test pulse to +20 mV. The voltage protocol is illustrated in the inset. Peak current amplitudes during test pulses were plotted as a function of the previous potential. Normalized steady-state inactivation–test potential relations were fitted to a Boltzmann function.

Table 1. Parameters of activation in currents expressing WT-HERG and/or A614V-HERG

	WT (2 μg) (n = 26)	WT (1 μg) (n = 22)	WT (1 μg) / A614V (1 μg) (n = 20)	A614V (2 μg) (n = 10)
Peak tail current (pA/pF)	43.2 ± 4.0	29.4 ± 3.4	7.9 ± 1.1**	0.6 ± 0.5**
$V_{0.5}$ (mV)	−20.6 ± 1.2	−20.8 ± 1.0	−22.7 ± 1.0	
k (mV)	7.6 ± 0.3	7.8 ± 0.2	7.1 ± 0.3	

**P<0.01 *vs* WT (1 μg).

Hydroxyzine inhibited both WT and WT/A614V HERG currents

In the next series of experiments, we examined whether hydroxyzine exerts inhibitory effects on reconstituted HERG currents to explain the drug-induced cardiac event in our index patient. Figure 4A shows a representative experiment to examine the effect of hydroxyzine on WT-HERG current. Current traces were measured before (left) and after (right) extracellular application of 1 μM hydroxyzine. Time-dependent outward current during depolarizing pulses as well as tail currents elicited on return to −60 mV were reduced by hydroxyzine. In Fig. 4, B and C, tail current and normalized tail current densities are plotted against test potentials (open circles: control and filled circles: 1 μM hydroxyzine). As depicted in Fig. 4B, hydroxyzine significantly decreased WT-HERG currents (P<0.01 *vs* WT-HERG, Table 2). Hydroxyzine also modified the voltage-dependence of activation of the WT-HERG channels and produced a significant shift of $V_{0.5}$ toward

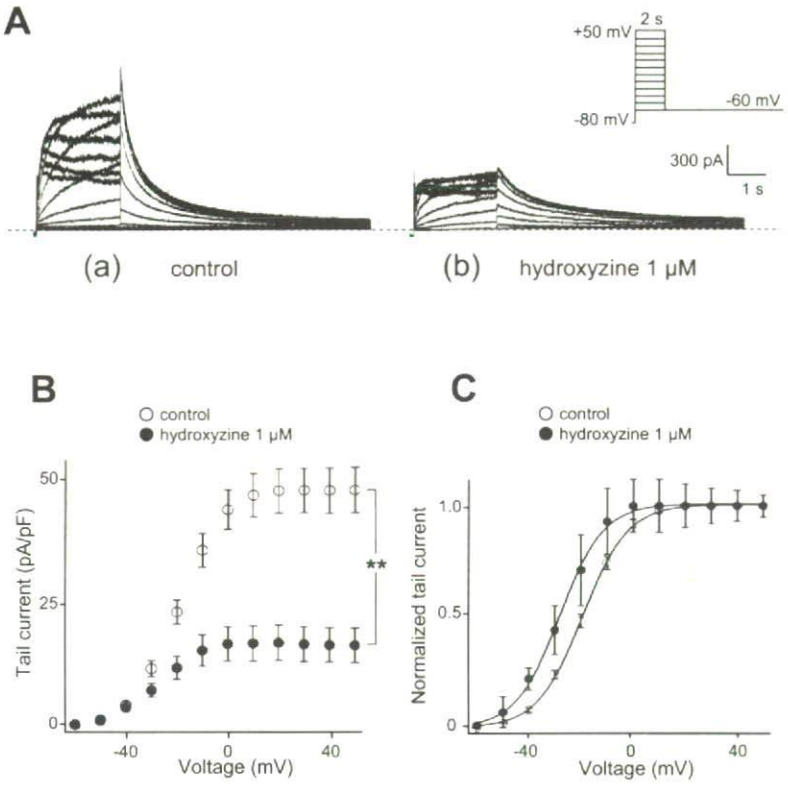

Fig. 4. Hydroxyzine block of WT-HERG K^+ currents. Representative current traces recorded in CHO cells expressing WT-HERG in control condition (a) and in the presence of hydroxyzine (1 μM) (b). Tail current–voltage relations for the control condition (open circles, n = 16) and in the presence of hydroxyzine (1 μM) (filled circles, n = 16). **P<0.01 *vs* WT-HERG. Normalized activation curves.

Table 2. Parameters of activation in currents in the presence of hydroxyzine (1 μM)

	WT (n = 16)	WT + hydroxyzine (1 μM) (n = 16)	WT/A614V (n = 13)	WT/A614V + hydroxyzine (1 μM) (n = 13)
Peak tail current (pA/pF)	45.1 ± 4.0	15.3 ± 3.3**	6.0 ± 0.9	2.1 ± 0.6**
$V_{0.5}$ (mV)	−19.9 ± 0.9	−26.7 ± 1.1**	−20.4 ± 1.2	−28.6 ± 2.4**
k (mV)	7.6 ± 0.3	7.9 ± 0.4	7.2 ± 0.3	6.1 ± 0.7

**P<0.01 *vs* control (absence of drug).

more negative potentials (Fig. 4C, Table 2). Similarly, HERG currents reconstituted by the co-transfection of WT and A614V were also significantly inhibited by hydroxyzine (Table 2 and see also Fig. 5A).

The drug sensitivity of HERG channel currents were extensively assessed by applying various concentrations of extracellular hydroxyzine under the whole-cell condition by means of the action potential command method (Fig. 5A). In the inset, the voltage-clamp protocol is shown, and the pulses with action potential configuration are given at 1 Hz. As shown in panel a of Fig. 5A, the compound (0.5 and 1 μM) inhibited WT (1 μg) HERG currents in a concentration-dependent manner (red trace: control, blue trace: 0.5 μM, and dark blue trace: 1 μM hydroxyzine).

Percent inhibitions of peak currents during action potential command waveforms were measured at six different concentrations of hydroxyzine and are plotted as a function of its concentrations (Fig. 5B, open circles). Smooth curves were drawn by fitting them to a Hill equation, yielding hydroxyzine a half maximum inhibitory concentration (IC_{50}) of 0.62 μM and Hill coefficient of 0.99.

We examined hydroxyzine concentration–inhibition relation for WT/A614V (1 μg each) HERG currents as conducted on WT currents. As shown in panel b of Fig. 5A, WT/A614V currents were also inhibited by micromolar concentrations of hydroxyzine. Its concentration–inhibition curve (Fig. 5B, filled circles) almost overlapped that observed in regard to WT-HERG currents. Fitting to a Hill equation yielded the IC_{50} of 0.52 μM and the Hill coefficient of 1.01. These values

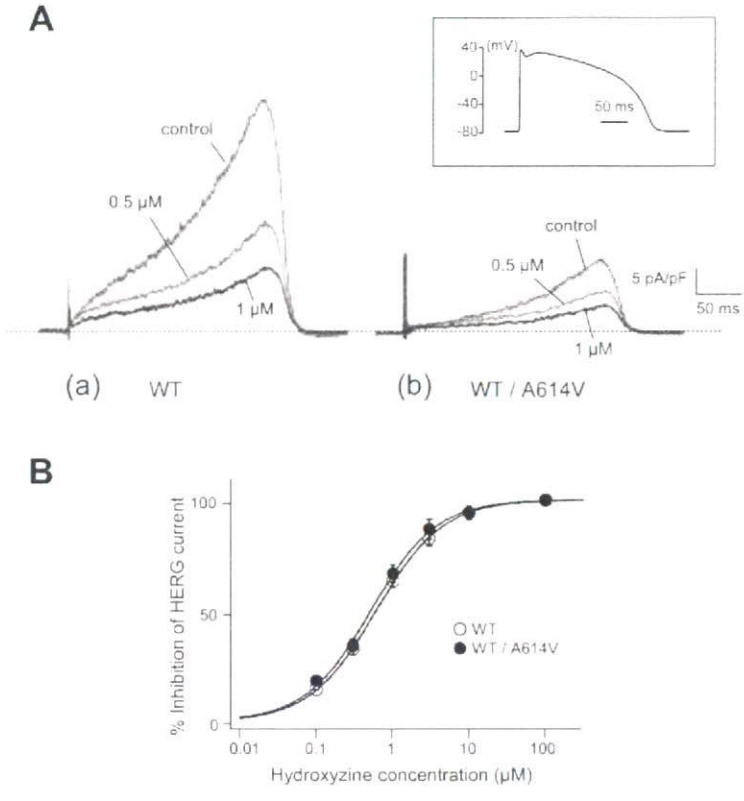

Fig. 5. Concentration-dependent block of both WT and WT/A614V HERG by hydroxyzine. Representative current traces recorded in CHO cells expressing WT HERG (a) and WT/A614V HERG (b) in control condition and in the presence of increasing hydroxyzine concentrations. An action potential wave form recorded from a cat ventricular myocyte was used as the command voltage to clamp. HERG currents are expressed as a normalized E-4031-sensitive current (control current – residual current in 3 μM E-4031). Dose–response curve for hydroxyzine to block WT and WT/A614V HERG K^+ current. Current was normalized to the control value and expressed as a function of the drug concentration. Solid line, fit of experimental data to the Hill equation: $y = a + \{d / [1 + (x/c)^{n_H}]\}$, where x is the drug concentration and n_H is the Hill coefficient. IC_{50} value was calculated as the drug concentration for which y = 50%.

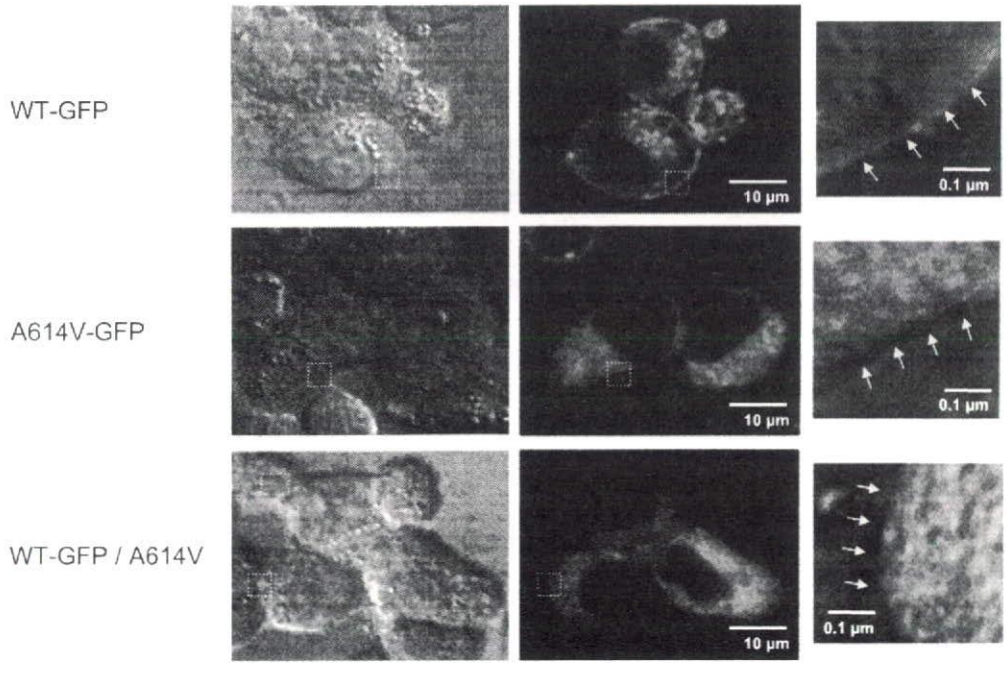

Fig. 6. Subcellular distribution of WT, A614V and WT/A614V in HEK293 cells. Representative microscopic images of HEK293 cells expressing GFP-tagged WT HERG (three upper panels), GFP-tagged A614V mutant (middle three), and GFP-tagged WT HERG co-transfected with non-tagged A614V mutant (lower three). The three panels in the left column show contrast microscopic images and the middle 3 panels, corresponding confocal microscopic images. The three panels in the right column display magnified images of yellow-boxed areas in the left and middle column panels. Yellow arrows on the images indicate the margin between the surface membrane and extracellular space.

were not statistically different from those obtained for WT-HERG currents.

We also examined the effect of hydroxyzine on KCNQ1/KCNE1 currents reconstituted in CHO cells. Hydroxyzine did not inhibit KCNQ1/KCNE1 currents at 1 μM concentration, and 10 μM of the drug only inhibited the KCNQ1/KCNE1 currents by $9 \pm 2.9\%$ (n = 8) (data not shown).

A614V HERG is a trafficking-deficient mutation

The results of electrophysiological experiments showed that hydroxyzine exerted a similar inhibitory effect on both WT and WT/A614V channel currents (Fig. 5) and that both types of channels showed a similar voltage-dependent activation process (Fig. 3). Using a Western blot analysis, Anderson et al. (15) demonstrated that A614V is a trafficking-deficient mutation. Collectively, the A614V mutant subunit appeared refractory to the intracellular transport, and all the expressed channels were WT. In order to examine the intracellular transport of WT and mutant HERG channels in more detail, we finally conducted confocal imaging experiments using GFP-tagged clones. Whole-cell patch-clamp experiments confirmed that the GFP-tagged WT clone (WT-GFP) could successfully generate a similar size of typical HERG currents in CHO cells (data not shown). The left column of Fig. 6 depicts three confocal images in HEK293 cells expressing GFP-tagged WT (upper), GFP-tagged A614V (A614V-GFP) alone (middle), and GFP-tagged WT with non-tagged A614V (WT-GFP /A614V) (lower). The panels in the left column show corresponding images taken by a phase-contrast microscope. The regions of interest are indicated by small squares in the merged and expanded images (right) of green fluorescence (middle) and light transmission (left). WT-HERG channels were amply transported to the cell surface membrane; in contrast, A614V channels failed to attain a position on the membrane surface (indicated by yellow arrows). GFP signal obtained from WT-HERG in cells co-transfected with non-tagged A614V (right lower panel) could be detected but only scantily in the cell surface membrane. Thus, the findings confirmed the electrophysiological results, suggesting that A614V may trap WT-HERG protein and thereby hinder its cell surface expression.

Discussion

In the present study, submicromolar concentrations of (<1 μM) hydroxyzine hydrochloride, a first generation H_1-receptor blocker, were found to inhibit reconstituted HERG K^+ currents. The drug is a classical antihistamine with antiallergic, antimuscarinic, and sedative actions and has also cardiac adverse effects such as abnormal ventricular repolarization (16). Wang et al. (17) reported that the drug prolonged the QT interval in an isolated feline heart, and Taglialatela et al. examined the effects of first-generation antihistamines, including hydroxyzine, on human neuroblastoma cells and *Xenopus* oocytes expressing HERG channel (18). Other first generation H_1-receptor blockers such as chlorpheniramine, pyrilamine, and diphenhydamine were also indicated to block the rapidly activating component of the delayed rectifier potassium current, I_{Kr} (19 – 21). More recently, newer H_1-receptor antagonists, terfenadine and astemizole, were withdrawn from the market because of TdP occurrence (5 – 9). These antagonists have been shown to inhibit cardiac I_{Kr} currents in a concentration-dependent manner with IC_{50} values of 0.35 – 0.45 μM (3, 21). The hydroxyzine IC_{50} for HERG currents (0.62 μM) in our study is close to its reported maximum serum concentration in humans (0.16 μM after a single oral dose of 0.7 mg/kg hydroxyzine), and the drug has a very long washout time ($t_{0.5}$ = 20 h) (22, 23). We should therefore pay attention to its potential adverse action on QT intervals. Taglialatela et al. (18) reported that hydroxyzine's IC_{50} for HERG in oocytes was 10.7 μM, which is far higher than normal therapeutic concentrations. The differences in IC_{50} may reflect different experimental conditions, and we think that our data are more clinically relevant.

Both cardiac and non-cardiac agents are known to cause acquired drug-induced LQTS (24) through the inhibition of HERG channel currents (4). Hydroxyzine does not inhibit I_{Ks} at its therapeutic concentration range. Marked QT prolongation and repetitive syncope in our index patient were therefore associated with hydroxyzine-induced inhibition of HERG currents. However, the patient had another potential for the life-threatening arrhythmia: heterozygous mutation of the HERG gene. The unexpected combination of two risk factors appeared to cause a severe phenotype in this specific case. On functional assessment, the gene variant was found to reduce native HERG currents to one-fourth, and hydroxyzine still blocked WT/A614V HERG currents with a similar potency. Thus, even lower serum concentration of hydroxzyine would have produced considerable QT prolongation and presumably TdP, which may be a cause of the patient's syncope.

In the functional study, the A614V HERG mutation identified in our patient showed dominant negative effects on WT-HERG channels without affecting parameters of activation and inactivation. Using Western blot analyses, Andersen et al. (15) also reported that A614V is a trafficking-deficient mutation. In accordance with this report, we showed that A614V caused

deficiency in intracellular transport (protein trafficking) to the cell surface membrane, by using the confocal imaging method. Our methods could confirm their results and directly show the location of targeted proteins and added more findings on the transporting process of these proteins, especially when co-expressed. Therefore, A614V subunit incorporation into normal assembly appeared to prevent its healthy traffic to the plasma membrane. Using a heterologous expression system with *Xenopus* oocytes, Nakajima et al. (25) demonstrated that A614V suppressed HERG current in a dominant-negative manner through the enhancement of inward rectification resulting from the shift in voltage dependence of HERG inactivation. The inconsistency of the results about the voltage dependence of the steady-state inactivation may due to the difference of the cells used for experiments.

Impaired trafficking of HERG protein is increasingly recognized as a leading cause of type 2 LQTS. For several trafficking-deficient HERG channels, incubation of cells at reduced culture temperatures or with HERG blockers has been shown to rescue the deficient transport (15). Concerning the A614V-HERG channel, both thapsigargin and E4031 failed to improve the protein processing (15). We also tested whether hydroxyzine rescued the channel trafficking, but no recovery was observed (data not shown).

In conclusion, QT-prolonging drugs usually require the presence of multiple risk factors to manifest life-threatening arrhythmias (1). In our patient, both genetic background and female sex are definite risk factors to trigger the QT prolongation. In addition, hydroxyzine intake produced a "double hit", leading to a reduction in cardiac "repolarization reserve" (26) and a severe phenotype, presumably TdP. Thus, genetic screening is of clinical importance not only for familial LQTS patients but also for patients with drug-induced QT prolongation. When possible genetic background is identified, the genetic analysis is especially necessary for the proband's family members to avoid unexpected drug-induced adverse actions. Based on our electro-pharmacological study, hydroxyzine should be avoided for patients with prolonged QT intervals and be included in the list of drugs (http://www.torsades. org/medical-pros/drug-lists/drug-lists.cfm) that prolong the QT interval and/or induce torsades de pointes ventricular arrhythmia.

Acknowledgment

We thank Ms. A. Ikeda for her excellent technical support. This study was supported by the grants from Ministry of Education, Culture, Sports, Science, and Technology Leading Project for Biosimulation and health sciences research grants (H18 – Research on Human Genome – 002) from the Ministry of Health, Labour, and Welfare, Japan (M. Horie).

References

1 Roden DM. Drug-induced prolongation of the QT Interval. N Engl J Med. 2004;350:1013–1022.
2 Suessbrich H, Waldegger S, Lang F, Busch AE. Blockade of HERG channels expressed in *Xenopus* oocytes by the histamine receptor antagonists terfenadine and astemizole. FEBS Lett. 1996;385:77–80.
3 Roy M, Dumaine R, Brown AM. HERG, a primary human ventricular target of the nonsedating antihistamine terfenadine. Circulation. 1996;94:817–823.
4 Taglialatela M, Castaldo P, Pannaccione A, Giorgio G, Annunziato L. Human ether-a-gogo related gene (*HERG*) K^+ channels as pharmacological targets: present and future implications. Biochem Pharmacol. 1998;55:1741–1746.
5 Monahan BP, Ferguson CL, Killeavy ES, Lloyd BK, Troy J, Cantilena LR Jr. Torsades de pointes occurring in association with terfenadine use. JAMA. 1990;264:2788–2790.
6 MacConnell TJ, Stanners AJ. Torsades de pointes complicating treatment with terfenadine. Br Med J. 1991;302:1469.
7 Mathews DR, McNutt B, Okerholm R, Flicker M, McBride G. Torsades de pointes occurring in association with terfenadine use. J Am Med Assoc. 1991;266:2375–2376.
8 Craft TM. Torsade de pointes after astemizole overdose. Br Med J. 1986;292:660.
9 Simons FE, Kesselman MS, Giddins NG, Pelech AN, Simons KJ. Astemizole-induced torsade de pointes. Lancet. 1988;10; 2(8611):624.
10 Tsuji K, Akao M, Ishii TM, Ohno S, Makiyama T, Takenaka K, et al. Mechanistic basis for the pathogenesis of long QT syndrome associated with a common splicing mutation in KCNQ1 gene. J Mol Cell Cardiol. 2007;42:662–669.
11 Tanaka T, Nagai R, Tomoike H, Takata S, Yano K, Yabuta K, et al. Four novel KVLQT1 and four novel HERG mutations in familial long-QT syndrome. Circulation. 1997;95:565–567.
12 Satler CA, Vesely MR, Duggal P, Geoffrey SG, Beggs AH. Multiple different missense mutations in the pore region of HERG in patients with long QT syndrome. Hum Genet. 1998;102:265–272.
13 Splawski I, Shen J, Timothy KW, Lehmann MH, Priori S, Robinson JL, et al. Spectrum of mutations in long-QT syndrome genes: KVLQT1, HERG, SCN5A, KCNE1, and KCNE2. Circulation. 2000;102:1178–1185.
14 Yang T, Snyders DJ, Roden DM. Rapid inactivation determines the rectification and $[K^+]_o$ dependence of the rapid component of the delayed rectifier K^+ current in cardiac cells. Circ Res. 1997;80:782–789.
15 Anderson CL, Delisle BP, Anson BD, Kilby JA, Will ML, Tester DJ, et al. Most LQT2 mutations reduce Kv11.1 (hERG) current by a class 2 (trafficking-deficient) mechanism. Circulation. 2006;113:365–373.
16 Hollister LE. Hydroxyzine hydrochloride: possible adverse cardiac interactions. Psychopharmacol Commun. 1975;1:61–65.
17 Wang WX, Ebert SN, Liu XK, Chen YW, Drici MD, Woosley

RL. 'Conventional' antihistamines slow cardiac repolarization in isolated perfused (Langendorff) feline hearts. J Cardiovasc Pharmacol. 1998;32:123–128.
18 Taglialatela M, Timmerman H, Annunziato L. Cardiotoxic potential and CNS effects of first-generation antihistamines. Trends Pharmacol Sci. 2000;21:52–66.
19 Khalifa M, Drolet B, Daleau P, Lefez C, Gilbert M, Plante S, et al. Block of potassium currents in guinea pig ventricular myocytes and lengthening of cardiac repolarization in man by the histamine H_1 receptor antagonist diphenhydramine. J Pharmacol Exp Ther. 1999;288:858–865.
20 Salata JJ, Jurkiewicz NK, Wallace AA, Stupienski RF 3rd, Guinosso PJ Jr, Lynch JJ Jr. Cardiac electrophysiological actions of the histamine H_1-receptor antagonists astemizole and terfenadine compared with chlorpheniramine and pyrilamine. Circ Res. 1995;76:110–119.
21 Taglialatela M, Pannaccione A, Castaldo P. Molecular basis for the lack of HERG K^+ channel block-related cardiotoxicity by the H_1 receptor blocker cetirizine compared with other second-generation antihistamines. Mol Pharmacol. 1998;54:113–121.
22 Simons FE, Simons KJ, Frith EM. The pharmacokinetics and antihistaminic of the H_1 receptor antagonist hydroxyzine. J Allergy Clin Immunol. 1984;73:69–75.
23 Simons KJ, Watson WT, Chen XY, Simons FE. Pharmacokinetic and pharmacodynamic studies of the H_1-receptor antagonist hydroxyzine in the elderly. Clin Pharmacol Ther. 1989;45:9–14.
24 Witchel HJ, Hancox JC. Familial and acquired long QT syndrome and the cardiac rapid delayed rectifier potassium current. Clin Exp Pharmacol Physiol. 2000;27:753–766.
25 Nakajima T, Furukawa T, Tanaka T, Katayama Y, Nagai R, Nakamura Y, et al. Novel mechanism of HERG current suppression in LQT2 shift in voltage dependence of HERG inactivation. Circ Res. 1998;83:415–422.
26 Roden DM, Yang T. Protecting the heart against arrhythmias: potassium current physiology and repolarization reserve. Circulation. 2005;112:1376–1378.

Circ J 2008; **72:** 687–693

A Novel Mutation Associated With Jervell and Lange-Nielsen Syndrome in a Japanese Family

Seiko Ohno, MD; Tomoyuki Kubota, MD; Hidetada Yoshida, MD; Keiko Tsuji, MS*; Takeru Makiyama, MD; Satsuki Yamada, MD**; Keisuke Kuga, MD**; Iwao Yamaguchi, MD**; Toru Kita, MD; Minoru Horie, MD*

Background The Jervell and Lange-Nielsen (JLN) syndrome is a variant of long QT syndromes (LQTS) and is associated with congenital deafness. The syndrome is caused by homozygous or compound heterozygous mutations in genes *KCNQ1* and *KCNE1*, which are responsible for encoding the delayed rectifier repolarizing current, I_{Ks}.

Methods and Results A novel and homozygous *KCNQ1* mutation in a 23-year-old deaf woman with a prolonged QT interval and recurrent syncope in a Japanese family was identified. Genetic analyses revealed that the proband harbored a *KCNQ1* missense mutation (W248F) located in the intracellular S4-S5 linker on both alleles. The same mutation was identified in both maternal and paternal families in a heterozygous manner. However, the family members of both sides had no clinical evidence of LQTS or hearing defects. Functional assays using a heterologous expression system revealed that W248F KCNQ1 plus KCNE1 channels reconstitute hardly measurable I_{Ks} currents. In contrast, heterozygous wild-type/W248F KCNQ1 plus KCNE1 channels displayed biophysical properties similar to those of the wild-type KCNQ1 plus KCNE1 channels with a weak dominant-negative effect.

Conclusion In this study, we present a family with JLN syndrome. The electrophysiological properties of the mutant I_{Ks} channels explain the pathophysiology underlying JLNS. (*Circ J* 2008; **72:** 687–693)

Key Words: Ion channel; Jervell and Lange-Nielsen syndrome; *KCNQ1*; Long QT syndromes; Molecular screening

The Jervell and Lange-Nielsen (JLN) syndrome is a variant of long QT syndromes (LQTS);[1] a rare clinical entity characterized by a prolonged QT interval on electrocardiograms (ECGs) and congenital bilateral deafness, which is the cause of sudden cardiac death during childhood and young adulthood.[2,3] In 1957, JLN presented a Norwegian family in which 4 of 6 siblings born to unrelated normal parents had prolonged QT intervals on ECGs and loss of hearing.[4] Four of the affected children had suffered from recurrent attacks of faintness occurring from early childhood, and 3 of them died suddenly at the ages of 4, 5, and 9 years, respectively. Cardiac symptoms are now known to result from a delayed repolarization of the cardiac action potential, which triggers polymorphic ventricular tachycardias, *torsade de pointes*. It terminates spontaneously or often degenerates into ventricular fibrillation,[5] and affected patients are known to have a very high mortality.[2,3] After the original report, an autosomal recessive mode of inheritance was suggested to be the cause in other independent cases with similar clinical findings; there was a high incidence of parental consanguinity among the affected families, and both parents of affected children were clinically normal.[6] There are, however, a few earlier descriptions of parents with subtle QT-interval prolongation in these same families.[6,7]

Regarding the genetic background of the JLN syndrome, homozygous or compound heterozygous mutations in *KCNQ1*[8,9] or *KCNE1*[10,11] have been identified, and these genes encode the K^+ channel subunits that are responsible for the slowly activating delayed rectifier K^+ current (I_{Ks}).[12,13]

More recently, we identified a Japanese family suffering from JLN syndrome, in which the index patient with QT prolongation and deafness (a 23-year-old woman) experienced severe and repeated attacks of syncope that were finally controlled by β-blockers. Conversely, other family members remained entirely healthy without QT prolongation.

Genetic testing revealed the proband, and 3 of the healthy family members from both the paternal and maternal side were found to have homozygous and heterozygous W248F mutations of *KCNQ1*. Compared to severe phenotypes in the index patient, a complete lack of JLN syndrome phenotypes was impressive in other genetically affected relatives. Because the clinical features of the family appeared to depend on the mutation of the causative gene, we conducted a functional assay of the W248F-KCNQ1/KCNE1 channel by using a heterologous expression system.

(Received May 28, 2007; revised manuscript received November 9, 2007; accepted December 10, 2007)

*Department of Cardiovascular Medicine, Kyoto University Graduate School of Medicine, Kyoto, *Department of Cardiovascular and Respiratory Medicine, Shiga University of Medical Science, Otsu and **Department of Internal Medicine, Institute of Clinical Medicine, Graduate School of Comprehensive Human Sciences, University of Tsukuba, Tsukuba, Japan*

Mailing address: Minoru Horie, MD, Department of Cardiovascular and Respiratory Medicine, Shiga University of Medical Science, Seta Tsukinowa-cho, Otsu 520-2192, Japan. E-mail: horie@belle.shiga-med.ac.jp

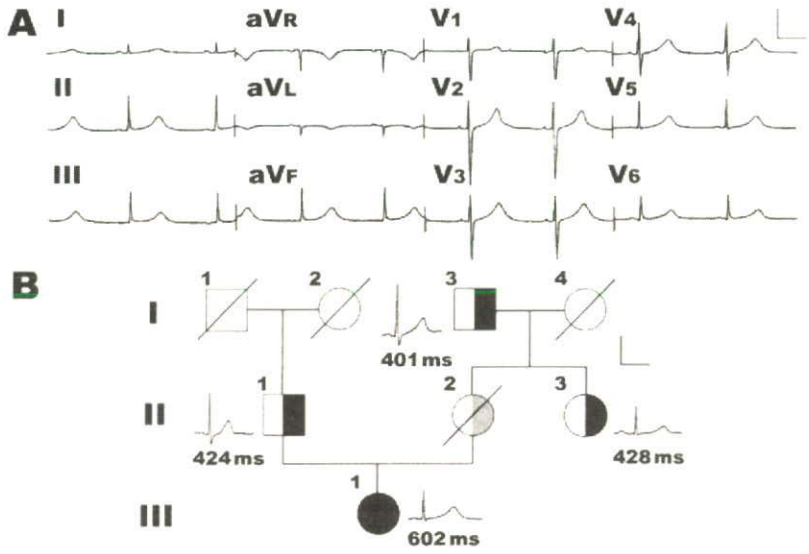

Fig 1. Twelve-leads electrocardiogram (ECG) of the proband and pedigree structure of the family with Jervell and Lange-Nielsen (JLN) syndrome. (A) This ECG demonstrating QT prolongation was obtained as part of a work-up to elicit the cause of recurrent syncope. Note broad-based T waves associated with prolonged QT intervals. (B) Roman numerals refer to the different generations and numbers 1 through 4 identify individuals within each generation. Circles indicate female family members, squares indicated male family members and slashes indicate deceased family members. The proband (III-1) is indicated by the solid circle representing the JLN syndrome, and the family members of mutation carrier indicated by half filled circle or squares. The mother of the proband, a obligate heterozygous carrier, is indicated by a gray colour. QTc intervals corrected by Bazzet's formula and associated ECG recordings in lead V5 are given for each available family member. Scale bars indicate 10 mA and 400 ms.

Methods

Subjects

The proband was identified in a small Japanese family without any known consanguinity and referred to our laboratory for genetic evaluation. Subjects gave their written informed consent in accordance with the guidelines approved by the appropriate institutional review boards. Each subject underwent detailed clinical and cardiovascular examinations, and then was characterized on the basis of the QT interval in lead V5, was corrected for heart rate (QTc) according to Bazett's formula and the presence of cardiac symptoms.

Mutation Analysis

Genomic DNA was isolated from peripheral blood lymphocytes of the proband and from family members by use of the QIAamp DNA blood midikit (Qiagen, Hilden, Germany). Previously published primer pairs[14] were used to amplify the entire coding regions of the known LQTS genes (*KCNQ1*, *KCNH2*, *SCN5A*, *KCNE1* and *KCNE2*) with the exception of *ANKB*,[15] *CAV3*[16] and *SCN4B*[17] from genomic DNA. Polymerase chain reaction (PCR)-single-strand conformation polymorphism (SSCP) analysis was performed at 2 temperatures, 6°C and 24°C, as described elsewhere.[18] PCR fragments presenting abnormal bands in SSCP analysis were subsequently sequenced using an ABI 3100 genetic analyzer (PE Applied Biosystems, Foster City, CA, USA).

Mutagenesis and Heterologous Gene Expression in CHO Cells

Complementary DNAs (cDNAs) for human *KCNQ1* (GenBank AF000571) and *KCNE1* (GenBank M26685) were sub-cloned into pIRES2-EGFP (for *KCNQ1*) and pIRES-CD8 (for *KCNE1*). The *KCNQ1* mutant was constructed using a Quick Change II XL Site-Directed Mutagenesis kit, according to the manufacturer's instruction (Stratagene, La Jolla, CA, USA). The nucleotide sequence of the construct was confirmed prior to the expression studies. CHO cells were transiently transfected using 1 μg of wild type (WT) or mutant pIRES2-EGFP/*KCNQ1*, and 1 μg of pIRES-CD8/*KCNE1* per 35 mm dish, using Fugene6 reagents (Roche Diagnostics, Basel, Switzerland). In some experiments, 0.5 μg of WT pIRES2-EGFP/*KCNQ1* was transfected with or without mutant pIRES2-EGFP/*KCNQ1*, instead of 1 μg of pIRES2-EGFP/*KCNQ1*. Cells successfully transfected with both *KCNQ1* and *KCNE1* cDNAs were selected by green fluorescence and decoration with anti-CD8 antibody-coated beads (Dynabeads CD8; Dynal Biotech, Oslo, Norway).

Electrophysiological Experiments and Data Analysis

Whole-cell mode of patch-clamp recordings was performed at 37°C by using an Axopatch 200A patch clamp amplifier (Axon Instruments, Foster City, CA, USA) 48 to 72 h after transfection. The pClamp software (version 9.0, Axon Instruments) was used to generate voltage pulse protocols and for data acquisition. The pipettes were filled with an internal solution (mmol/L) made up of the following: KCl 130, KOH 20, Mg-ATP 5, Na-GTP 0.1, EGTA 5 and HEPES 10 (pH 7.2 with KOH), and had a resistance of 2.0 to 4.0 mol Ω. The solution used to perfuse the cells contained (in mmol/L): NaCl 140, KCl 5.4, $MgCl_2$ 0.5, $CaCl_2$ 1.8, NaH_2PO_4 0.33, glucose 5.5, and HEPES 5 (pH 7.4 with NaOH). Data was filtered at 2 kHz.

Activation curves were derived from tail currents at –40 mV after testing potentials ranging from –60 to +60 mV, or –60 to +120 mV. Current-voltage relations were fitted with a Boltzmann's function:

$$I_{K,tail} = 1/(1+\exp((V_{1/2}-V_m)/k)) \qquad (Eqn\ 1)$$

where $V_{1/2}$ is the potential at which the activation is half-maximal, V_m is the test potential and k is the slope factor.

Numerical data was presented as mean ± standard error. Statistical analysis was performed using an ANOVA, followed by a Tukey-Kramer post hoc comparison. Statistical significance was set at $p<0.05$.

Results

Phenotypic Characterization

A 23-year-old woman was clinically diagnosed with JLN syndrome. She was congenitally deaf and had experienced several episodes of syncope since the age of 6 years. Her resting ECG showed a prolonged QT interval (Fig 1A). Episodes of syncope were most often elicited by physical stress, especially swimming, but cardiac resuscitation had

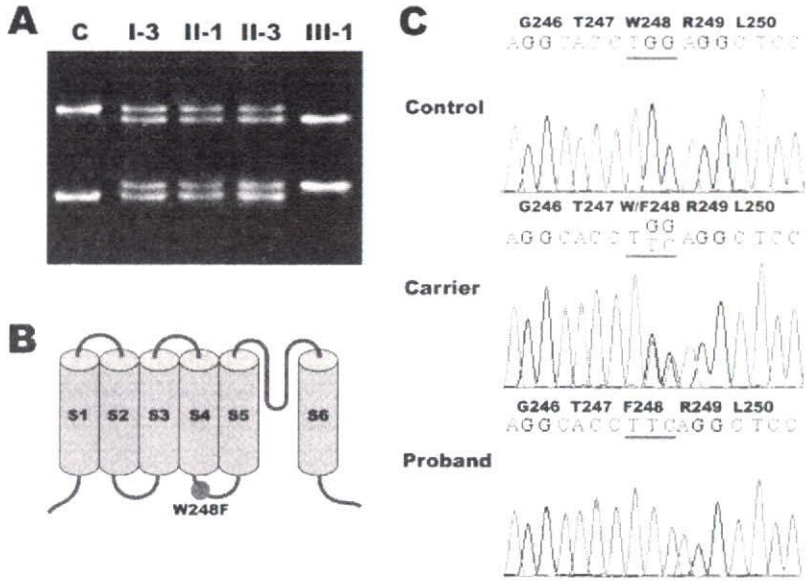

Fig 2. Single-strand conformation polymorphism (SSCP) and sequence analyses of KCNQ1. (A) SSCP analyses of polymerase chain reaction products amplifying exon 5; the control (C) shows a normal migration pattern. The family members (I-3, II-1, II-3) show normal and additional band patterns, and the proband (III-1) shows only an additional band pattern. (B) A schema of the KCNQ1 channel shows the location of the W248F-KCNQ1 mutation. (C) Sequence analyses in exon 5 of the control (Upper panel), and a family member who is a mutation carrier (Middle panel) and the proband (Lower panel) reveal G-to-T and G-to-C substitutions at position 743-744 (W248F). Numbering of the deduced amino acids is given according to Gene Bank cDNA: AF000571.

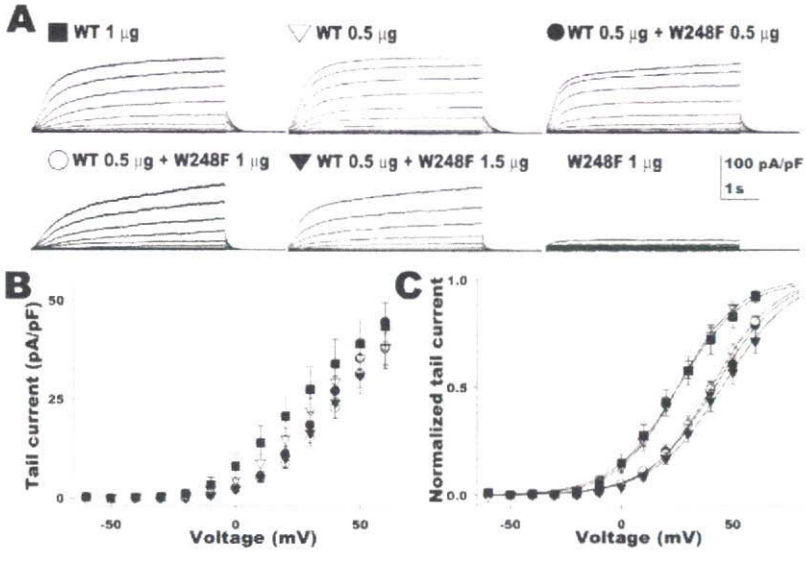

Fig 3. Functional analysis of wild type (WT) and/or W248F-KCNQ1 I_{Ks} channels expressed in CHO cells. (A) Representative current recordings. Currents were elicited from a holding potential of −70 mV, by depolarizing pulses (5-s duration) from −60 to +60 mV (with a 10-mV step increment) and subsequent repolarization to −40 mV for a 2-s duration. Concentrations of cDNAs used for transfection (volume/dish) are indicated above each graph. (B) Tail current-voltage relationships for 1 μg WT (closed square; n=13), 0.5 μg WT (open triangles; n=19), 0.5 μg WT+0.5 μg W248F (closed circle; n=21), 0.5 μg WT+1 μg W248F (open circles; n=23) and 0.5 μg WT+1.5 μg W248F (closed triangles; n=23). (C) Normalized activation curves by fitting to Boltzmann's equation (*Eqn 1*).

never been required. At the age of 21 years, β-blocker therapy was initiated with oral propranolol (0.8 mg·kg^{-1}·day^{-1}). After that, the woman remained symptom-free for a period of 2 years. A Holter 24-h ECG recording demonstrated relatively prolonged QTc intervals at fast heart rates, but no ventricular arrhythmia was observed.

Clinical manifestations of available family members were completely unremarkable. None of the family members had prolonged QTc intervals (indicated in Fig 1B with ECG monitors), experienced any symptoms compatible with LQTS, nor reported hearing deficits. There was no family history of sudden cardiac death; proband's mother (II-2), maternal grandmother (I-4) had died of rectal cancer and gastric cancer at the age of 35 and 82 years, respectively, and paternal grandparents (I-1, I-2) died from a stroke at the age of 74 and 85 years, respectively.

Mutation Analysis

SSCP analyses of *KCNQ1* revealed an abnormal migration pattern at exon 5 in the proband (Fig 2A). The abnormal pattern resulted from 2 homozygous nucleotide changes (743G>T and 744G>C) in exon 5 causing an amino acid substitution denoted W248F. This results in the replacing of a tryptophan at residue 248 with a phenylalanine, located in the intracellular S4-S5 linker (Figs 2B,C). This particular anomaly was absent in 220 alleles from 110 healthy individuals from the general population that were unrelated to the family. To exclude the possibility of a coincidental occurrence of LQTS and deafness, we extensively examined all other LQTS-related genes, but no additional mutations were identified. The proband's father (II-1), maternal aunt (II-3) and maternal grandfather (I-3) had the same W248F *KCNQ1* mutations in a heterozygous manner (Figs 2A,C). Although the proband's mother who died from rectal cancer was free of LQTS-related symptoms, she was considered to be an obligate heterozygous carrier of W248F.

Characterization of the Biophysical Properties of W248F KCNQ1

To assess the functional consequence of W248F *KCNQ1*,

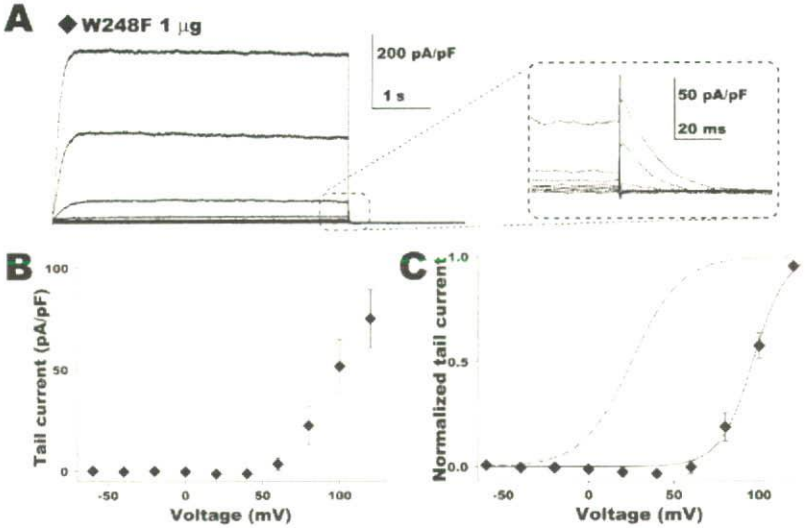

Fig 4. Functional analysis of W248F-KCNQ1 I_{Ks} channels expressed in CHO cells. (A) A representative current recording. The current was elicited from a holding potential of –70 mV, by depolarizing pulses (5-s duration) from –60 to +120 mV (with a 20-mV step increment) and subsequent repolarization to –40 mV for a 2-s duration. The small tail current in the dotted box was expanded. Note the outward currents and extremely rapid deactivation after depolarization to +80 ~ +120 mV. (B) Tail current-voltage relationships. Each symbol represents mean data obtained from 12 cells. Vertical bars indicate standard error. (C) Normalized activation curve by fitting to Boltzmann's equation (*Eqn 1*). The dashed line indicates the 1 μg wild type I_{Ks} channel displayed in Fig 3C.

Table 1 Summary of KCNQ1 Mutations in JLN Syndrome

Nucleotide change	*Amino acid change*	*Region*	*Mutation type*	*Symptom of the carriers*	*QTc of the carriers*	*References*
451–452delCT	*A150fs+132*	*S2*	*FS/del*	*None*	*N*	*25*
477+1 G>A	*M159sp*	*S2*	*SE*	*None*	*N*	*26, 27*
*477+5 G>A**	*M159sp*	*S2*	*SE*	*None*	*N, B, P*	*28*
*C513G**	*Y171X*	*S2-S3*	*NS*	*None*	*N, B*	*29, 30*
567insG	*G189fs+94*	*S2-S3*	*FS/ins*	*Syncope, SD*	*B, P*	*9*
572-576del†	*L191fs+90*	*S2-S3*	*FS/del*	*Syncope*	*N, B, P*	*20, 31, 32*
*585delG**	*R195fs+40*	*S2-S3*	*FS/del*	*None*	*N*	*30*
*G604A**	*D202N*	*S3*	*MS*	*None*	*B, P*	*30*
G728A†	*R243H*	*S4-S5*	*MS*	*Unknown*	*N, B*	*28, 31*
G743T-G744C	*W248F*	*S4-S5*	*MS*	*None*	*N*	*This study*
G783C	*E261D*	*S4-S5*	*MS*	*None*	*N*	*32, 33*
*G806A**	*G269D*	*S5*	*MS*	*None*	*N, B, P*	*30*
G914C	*W305S*	*Pore*	*MS*	*None*	*N, B*	*34*
1008delC	*A336fs+16*	*S6*	*FS/del*	*None*	*N*	*33*
1188delC	*I396fs+21*	*C-term*	*FS/del*	*Unknown*	*Unknown*	*35*
C1552T†	*R518X*	*C-term*	*NS*	*Normal*	*N,B*	*20, 32, 35, 36*
C1588T†	*Q530X*	*C-term*	*NS*	*None*	*N*	*4, 32, 33*
1630 del6/ins7	*E543fs+107*	*C-term*	*FS/del/ins*	*None*	*N, B, P*	*8*
*C1760T**	*T587M*	*C-term*	*MS*	*No carrier*	*No carrier*	*37*
G1766A†	*G589D*	*C-term*	*MS*	*None*	*N, B, P*	*29*
*G1781A**	*R594Q*	*C-term*	*MS*	*None*	*N*	*33*
*1892del20**	*P630fs+13*	*C-term*	*FS/del*	*None*	*N*	*37*

JLN, Jervell and Lange-Nielsen; del, deletion; fs, last amino acid unaffected by a frame shift (number after fs is the number of amino acids before termination); FS, frameshift; N, normal QTc <450 ms; sp, last unaffected amino acid before predicted splice mutation; SE, splice error; B, borderline QTc 450–480 ms; P, prolonged QTc >480 ms; NS, nonsense mutation; ins, insertion; SD, sudden death; MS, missense mutation.

**All cases and †some cases have compound heterozygous mutations.*

we co-expressed WT and W248F *KCNQ1* with the *KCNE1* gene, which encodes the accessory protein of the KCNQ1 channel. Fig 3A shows representative I_{Ks} current traces recorded from a CHO cell transfected with WT or W248F *KCNQ1* plus *KCNE1*. CHO cells transfected with WT-*KCNQ1* (1 or 0.5 μg, Fig 3A Upper left 2 panels) displayed outward currents with slow activation/deactivation kinetics on the prolonged depolarization (5-s in duration), which are typical of I_{Ks} currents, as previously reported.[12,13] In contrast, a cell transfected with W248F-*KCNQ1* (1 μg; Fig 3A Lower right panel) displayed hardly measurable I_{Ks} currents when depolarized to +60 mV. Co-expression of WT and W248F at an equimolar ratio (0.5 μg each; Fig 3A Upper right panel), mimicking the heterozygous inheritance, produced an intermediate size of outward currents resembling a WT I_{Ks} channel. To investigate the dominant-negative effect of W248F-*KCNQ1*, we further recorded the currents with co-expression of WT and W248F at 1:2 or 1:3 ratios. Both of the currents also resembled those of WT.

In Fig 3B, the tail current densities at –40 mV measured in multiple cells are plotted as a function of test pulse voltage (between –60 and +60 mV). The tail current densities after depolarizing the test pulse to +40 mV were 34.0± 6.2 pA/pF for 1 μg WT (n=13), 29.4±4.1 pA/pF for 0.5 μg WT (n=19), 27.0±3.8 pA/pF for 0.5 μg WT plus 0.5 μg W248F (n=21), 22.7±2.6 pA/pF for 0.5 μg WT plus 1 μg W248F (n=23) and 24.1±4.1 pA/pF for 0.5 μg WT plus 1.5 μg W248F (n=23). Thus, compared to the WT I_{Ks}